Combustion and Flame 181 (2017) 198–213

Contents lists available at ScienceDirect

Combustion and Flame

journal homepage: www.elsevier.com/locate/combustflame

An extensive experimental and modeling study of 1-butene oxidation

Yang Li, Chong-Wen Zhou, Henry J. Curran*

Combustion Chemistry Centre, National University of Ireland, Galway, Ireland

ARTICLE INFO

Article history:
Received 12 January 2017
Revised 16 February 2017
Accepted 21 March 2017
Available online 13 April 2017

Keywords:
1-Butene
Shock tube
Rapid compression machine
Chemical kinetics
Ignition delay time

ABSTRACT

In this study, a series of ignition delay time (IDT) experiments of 1-butene were performed in a high-pressure shock tube (HPST) and in a rapid compression machine (RCM) under conditions of relevance to practical combustors. This is the first 1-butene IDT data taken at engine relevant conditions, and the combination of HPST and RCM results greatly expands the range of data available for the oxidation of 1-butene to higher pressures (10–50 atm), lower temperatures (670–1350 K) and to a wide range of equivalence ratios (0.5–2.0).

A comprehensive chemical kinetic mechanism to describe the combustion of 1-butene has simultaneously been applied. It has been validated using the IDT data measured here in addition to a large variety of literature data: IDTs, speciation data from jet-stirred reactor (JSR), premixed flame, and flow reactor, and laminar flame speed data. Important reactions have been identified via flux and sensitivity analyses including: (a) H-atom abstraction from 1-butene by hydroxyl radicals and molecular oxygen from different carbon sites; (b) addition reactions, including hydrogen atom and hydroxyl radical addition to 1-butene; (c) allylic radical chemistry, including the addition reactions with methyl radical, hydroperoxy radical and self-recombination; (d) vinylic radical chemistry, including the addition reaction with molecular oxygen; (e) alcohol radical chemistry, including the Waddington type propagating reaction pathways and alkyl radical low-temperature branching chemical pathways.

1. Introduction

Alkenes are important intermediates formed during the combustion of larger hydrocarbons and alcohols. Moreover, liquefied petroleum gas (LPG) produced during oil refining contains a significant quantity of alkenes, particularly propene and butenes [1], with gasoline fuel containing butenes, pentenes, and hexenes in various amounts. Butene is the shortest alkene with structural isomers including, isobutene, 1-butene, cis-2-butene, and trans-2-butene. 1-butene is the smallest unsaturated hydrocarbon having a secondary allylic carbon group and a primary carbon group which exhibit both alkane- and alkene-type chemistry.

There have been some high-temperature and low-pressure experimental and kinetic modeling studies of 1-butene consumption, including pyrolysis and oxidation. The types of reactors and conditions studied are shown in Table 1.

Most recently, Zhao et al. [9] developed a high temperature kinetic model for the four butene isomers (1-, trans-2-, cis-2-, and isobutene) validated using laminar flame speeds and non-premixed counter-flow ignition temperatures at pressures of 2, 5, and 10 atm. Furthermore, the critical reaction paths for butene isomer oxidation during the induction period for ignition, particularly the allylic H-atom abstractions by ȮH radical, were systematically updated with rate coefficients from *ab-initio* calculations and kinetic theory.

Schenk et al. [7] studied premixed, low-pressure (40 mbar), flat, argon-diluted (25%) flames of three of the butene isomers (1-, trans-2-, and isobutene) under fuel-rich ($\varphi = 1.7$) conditions. This was the first detailed flame study of the butene isomers performed under fuel-rich conditions. The isomer-specific species information and the quantitative mole fraction profiles of more than 30 stable and radical species were measured using a newly developed analytical combination of high-resolution in-situ molecular-beam mass spectrometry (MBMS) and *in-situ* gas chromatography (GC), and it was used to validate and improve the subset of C_4 kinetics in a general hydrocarbon oxidation mechanism based on the work of Hoyermann et al. [10].

Zhang et al. [6] measured product and intermediate concentrations during the pyrolysis of 1-, 2-, and isobutene using synchrotron vacuum ultraviolet photoionization mass spectrometry (SVUV-PIMS) with the molecular-beam sampling technique in the temperature range 900–1900 K at a pressure of 3 Torr. Based on the experimental results, a kinetic model consisting of 76 species and

* Corresponding author.
E-mail address: henry.curran@nuigalway.ie (H.J. Curran).

http://dx.doi.org/10.1016/j.combustflame.2017.03.023
0010-2180/

Table 1
List of experimental literature data for 1-butene pyrolysis and oxidation.

No.	Reactor	φ	Diluent (%)	T (K)	p (atm)	References
1	Shock tube	0.5, 1.0, 2.0	87.0–96.0 (Ar)	1000–1700	1.2, 4.0, 16.0	Pan et al. [2]
2	Shock tube	0.5, 1.0, 2.0	87.0–96.0 (Ar)	1200–1670	6.6–8.9	Heyberger et al. [3]
3	Combustion vessel	0.7–1.4	75.31–77.11	–	1	Fenard et al. [4]
4	Jet-stirred reactor	0.25, 0.5, 1.0, 2.0	97.5–99.6	900–1440	1	Fenard et al. [4]
5	Jet-stirred reactor	0.15, 1.0, 4.0	90.0–93.85	900–1200	1.0–10.0	Chakir et al. [5]
6	Flow reactor	∞	96.0 (Ar)	900–1900	0.004–0.016	Zhang et al. [6]
7	Flame burner	1.7	25.0 (Ar)	2204	0.04	Schenk et al. [7]
8	Counterflow	0.7–1.7	74.6–77.1	2329	1.0, 2.0, 5.0, 10	Davis et al. [8]
9	Counterflow	–	–	1000–1300	1.0–5.0	Zhao et al. [9]

232 reactions was also developed to simulate the measured species mole fractions.

Fenard et al. [4] conducted experiments for the oxidation of 1- and cis-2-butene in a jet-stirred reactor and in a combustion vessel. The concentration profiles of stable species were measured in the temperature range 900−1440 K, at atmospheric pressure, for different equivalence ratios ($0.25 \leq \varphi \leq 2$). Laminar burning velocities were determined at $p = 1$ atm, at unburned gas temperatures in the range of 300–450 K, and at equivalence ratios in the range 0.8–1.4. A chemical kinetic mechanism based on a previously proposed scheme for the oxidation of hydrocarbons was also used to reproduce their experimental data (201 species involved in 1787 reactions).

Pan et al. [2] measured IDTs of 1-butene oxidation at pressures of 1.2, 4.0, and 16.0 atm, in the temperature range 1000–1700 K, and at equivalence ratios of 0.5, 1.0, and 2.0 in 87–96% argon diluent. Three widely used models, NUIG AramcoMech1.3 [11], USC Mech 2.0 [12] and the LLNL C4 [13] model were used to simulate the measured ignition delay times. It was found that none of the models could satisfactorily reproduce the experimental data, especially at lower temperatures.

Chakir et al. [5] measured the concentrations of molecular species produced from the oxidation of 1-butene in a jet-stirred reactor in the temperature range 900–1200 K, at pressures extending from 1 to 10 atm, for a wide range of fuel–oxygen equivalence ratios (0.15–4.0). A chemical kinetic reaction mechanism developed previously [14, 15] was used to simulate the experimental data.

Heyberger et al. [3] automatically generated a kinetic model for 1-butene using EXGAS, and it was used to simulate two sets of experimental results: species measurements in a jet-stirred reactor between 900 and 1200 K [5], and IDT measurements in a ST at temperatures in the range 1200–1670 K, at pressures from 6.6 to 8.9 atm, equivalence ratios from 0.5 to 2.0, using argon as bath gas.

There is still a lack of experimental data for 1-butene oxidation available in the literature at engine relevant, high-pressure, and low-temperature conditions. In addition, based on previous work on propene [16, 17], isobutene [18], and 2-butene [19], a comprehensive kinetic model for 1-butene oxidation will extend our understanding on alkene combustion chemistry.

In view of the above considerations, we have measured ignition delay times in a high-pressure shock tube (HPST) and in a rapid compression machine (RCM) at low temperatures (600–1000 K) and high pressures (>10 atm), which are of direct relevance to gasoline, diesel, and low-temperature combustion (LTC) engine technologies. In this work a comprehensive chemical kinetic mechanism to describe 1-butene oxidation has been developed, including detailed low-, intermediate- and high-temperature reaction pathways specific to unsaturated fuel chemistry. The model has been validated against a wide range of ignition delay time measurements from this work, the speciation and flame speed results from jet-stirred reactor, flow reactor, flame in the literature.

Table 2
Percentage molar composition of 1-butene mixtures.

	Fuel	O_2	Diluent	φ	p (atm)
1-butene	1.72	20.64	77.64	0.5	10, 30, 50
	3.38	20.29	76.33	1.0	10, 30, 50
	6.54	19.63	73.83	2.0	10, 30, 50

2. Experimental methods

IDT measurements for 1-butene were performed in a HPST and in an RCM located at NUI Galway (NUIG). Table 2 provides the detailed experimental conditions investigated in the present study. All fuels were acquired from Sigma Aldrich at 99.5% purity. Oxygen, nitrogen, argon and carbon dioxide were acquired from BOC Ireland at high purity (≥99.5%).

2.1. NUIG HPST

The HPST at NUIG was used to measure IDT for 1-butene at intermediate to high temperatures (~900–1300 K) at 10, 30, and 50 atm. The tube has an inner diameter of 63.5 mm, a 3 m driver section, a 5.7 m driven section, and a 3 cm double diaphragm section that is located between the driver and driven sections. Two pre-scored aluminum diaphragms are placed in the double-diaphragm section, and used to initiate the incident shock wave.

As to the diagnostic system, six PCB 113B24 pressure transducers are mounted in the sidewall of tube at known positions. The shock velocity at the end-wall is calculated by linearly extrapolating the five velocities to the end-wall. A Kistler 603B pressure transducer is mounted in the end-wall to measure the pressure versus time history behind the reflected shock wave. The IDT is defined as the interval between the rise in pressure due to the arrival of the shock wave at the end-wall and the rapid rise in pressure due to the ignition event, as shown in Fig. 1.

Post-shock conditions were determined using the normal shock relations as employed by Gaseq [20] utilizing measurements of incident shock velocity, initial temperature and pressure, and the thermodynamic properties of the shock-heated fuel/oxidizer mixtures. More detailed information can be found in a previous paper [21].

As to the uncertainty quantification of IDT measurements in our HPST, it has been reported by Petersen et al. [22] that the uncertainty of the reflected shock temperature is mainly attributable to the uncertainty of the incident shock velocity, which is determined by the uncertainties in the precise positions of the pressure transduces and the shock pass time recorded by the signal relayed to the oscilloscope from the pressure transducers. We have adopted a standard rt-sum-squares (RSS) method used by Petersen et al.

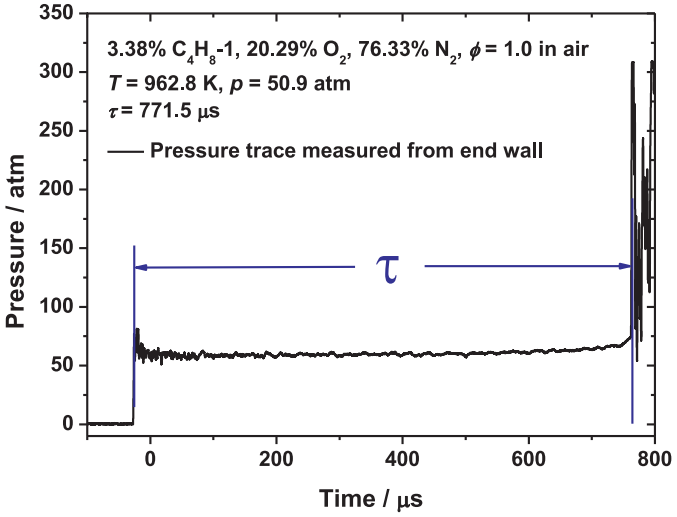

Fig. 1. A typical pressure–time history measured in the HPST.

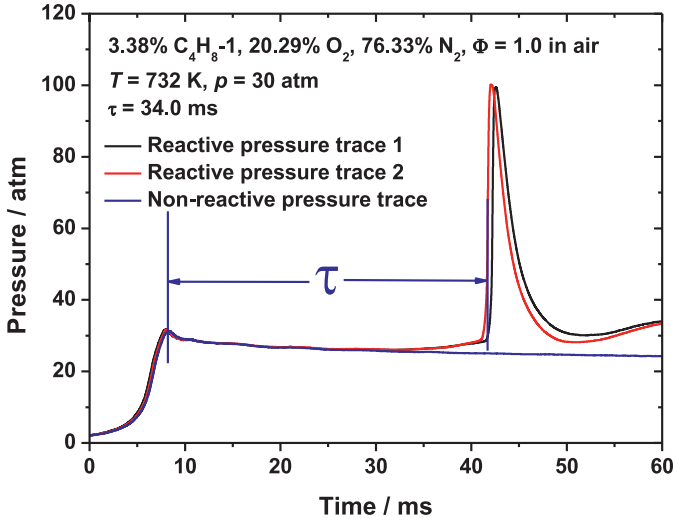

Fig. 2. A typical pressure–time history measured in the RCM.

[22],

$$T_5 = \frac{T_1\left[2(\gamma-1)M^2+(3-\gamma)\right]\left[(3\gamma-1)M^2-2(\gamma-1)\right]}{(\gamma+1)^2M^2}$$
$$= AM^2 + B + CM^{-2}$$
$$\mathrm{M} = \frac{V_s}{\sqrt{\gamma RT_1}}$$
$$\delta V_s = \sqrt{\left(\frac{1}{\Delta t}\delta_{\Delta z}\right)^2 + \left(\frac{-\Delta z}{\Delta t^2}\delta_{\Delta t}\right)^2}$$
$$\delta T_5 = \frac{\partial T_5}{\partial M}\delta M = \left(2AM - 2CM^{-3}\right)\frac{\delta V_s}{\sqrt{\gamma_1 RT_1}}$$

where T_5 is the reflected shock temperature (K); T_1 is the initial temperature (K); γ is the adiabatic exponent; V_s is the velocity of the incident shock wave ($\mathrm{m\,s^{-1}}$); and R is the gas constant. The uncertainty of the time intervals recorded using the six PCB 113B24 pressure transducers in our HPST and relayed to the TiePie Handyscope HS4 oscilloscope were estimated to be 1 μs, which corresponds to the sampling rate of the pressure transduce and the oscilloscope. The uncertainty in distance between the pressure transducers is estimated to be ±0.1 mm that stems mainly from the shock front thickness and the diameter of the sensing area of the pressure transducers. Using the above equations, the largest uncertainty in the reflected temperature is estimated to be 20 K. However, this uncertainty of the reflected shock temperature leads to a 20% uncertainty in measured ignition times, τ_{ign}, based on an Arrhenius-type correlation using the RSS method, a detailed description of which can be found in a previous study by Zhang et al. [23].

2.2. NUIG RCM

A clone of the original NUIG twin-opposed piston RCM was used in this study, and has been described previously [24]. The twin-opposed piston results in a short compression time of approximately 16 ms while the use of creviced piston heads leads to a homogeneous post-compression temperature distribution in the combustion chamber [25]. These piston heads achieve an approximate compression ratio of 12.5:1.

Different compressed gas temperatures are achieved by either varying the diluent gas composition or initial temperatures based on the adiabatic compression/expansion equation:

$$\ln\left(\frac{p_c}{p_i}\right) = \int_{T_i}^{T_c}\frac{\gamma}{\gamma-1}\frac{dT}{T}$$

where p_i is the initial gas pressure, p_C is the compressed gas pressure, T_i is the initial gas temperature, T_C is the compressed gas temperature and γ is temperature dependent ratio of specific heat.

Pressure–time profiles are measured using a Kistler 6045A pressure transducer, and the compressed gas pressure in above equation is taken as the pressure at the end of compression. The ignition delay time is measured from the first local maximum in the pressure–time history to the maximum rate of pressure rise due to ignition, as shown in Fig. 2. The reactive pressure traces 1 and 2 show the repeatability of our pressure measurements from two similar experiments.

In order to take heat loss effect into account, a non-reactive experiment, in which O_2 is replaced by an equivalent amount of N_2 in the mixture, was performed for every reactive experiment under the same conditions. For model simulations, non-reactive pressure–time profiles were converted to an "effective volume" history, which is then used as input file in CHEMKIN-PRO [26].

We have explored the uncertainty quantification of IDT measurements in an RCM in a previous study of isobutene oxidation [18]. We also recognize that uncertainty quantification for experimental data is an essential step in assessing the agreement between experimental data and kinetic mechanism simulation results. It is natural to think in terms of two types of uncertainties for RCM experiments; uncertainties in the measured ignition delay time, and uncertainties in the measured and inferred thermodynamic state of the reacting gas.

Ignition delay times can be measured quite accurately in the RCM. The high natural frequency of the transducer (80 kHz) used to monitor in-cylinder pressure along with the sufficient time-resolution of the data acquisition unit (20 kHz) permits the capture of both the end of compression time and the occurrence of the ignition event to within approximately 50 μs. The a-synchronicity of the pistons' arrival at maximum compression in our dual-piston machine contributes to shot-to-shot scatter in ignition delay measurements due to the stochastic change in piston seating. This a-synchronicity can cause inconsistencies for the defined end of compression time between reactive and non-reactive traces of up to 0.5 ms, which only induces large uncertainties when comparing experimental and simulated ignition delay times for short ignition

events (for example, ±5% for an ignition delay of 5 ms and ±0.5 at 50 ms).

While the RCM is accurate in recording ignition delay measurements, the characterization of the thermodynamic state of the reacting gas is more difficult, especially with regard to compressed temperatures that are evaluated from the adiabatic core hypothesis. Initial mixture mole fractions are expected to be accurate to within about ±2% of their reported nominal value, where the main contribution of uncertainty comes from partial pressure measurements. Time resolved measurements of in-cylinder pressures are readily achievable with modern static and dynamic pressure transducers, which result in the measurement of the initial reactor pressure and transient pressure history to within approximately ±0.05% and ±1 bar, respectively. Assuming perfect applicability of the adiabatic core hypothesis to the experiments conducted in this study and accounting for both uncertainties in the initial temperature and pressure measurements, the uncertainty of the inferred adiabatic core compressed temperature is less than approximately ±15 K.

3. Simulation methods

3.1. Ignition delay time simulations

Shock tube ignition delay time simulations were performed assuming a zero-dimensional, constant-volume reactor. The reflected shock pressure (p_5) and temperature (T_5) were used as the initial pressure and temperature, respectively. The non-ideal facility effect (dp/dt) for the reflected shock wave was found to be less than 2%/ms. However, due to the longer IDTs measured by Pan et al. [2] a $dp/dt = 4\%$ was taken into account for the simulations of their data presented as Supplementary material. For simulations of ignition delay time results already presented in the literature, the definition of ignition delay time is taken consistent with the particular diagnostic used in the reported experiments.

In simulating the rapid compression machine experiments an "adiabatic core expansion" approach [27–29] was employed, which accounts for the heat loss effect by adopting the volume–time history as discussed in Section 2.2.

3.2. Species simulations

Simulations of species measurements recorded in jet-stirred reactor, flow reactor and pre-mixed flame experiments were performed using the Perfectly Stirred Reactor (PSR), Plug Flow Reactor (PFR) and Premixed Laminar Burner-Stabilized Flame modules in CHEMKIN-PRO [26]. Pressure-distance and temperature-distance profiles from the experiments [6,7] are used as input files.

3.3. Flame speed simulations

Flame speed simulations were performed using the Premixed Laminar Flame-Speed simulator in CHEMKIN-PRO [26]. In order to avoid a high computational cost, a high-temperature version of the model was used to simulate the flame speed, which was created by removing all of the species and reactions involving low temperature oxidation chemistry, which is discussed in the following section.

3.4. Sensitivity analyses

Sensitivity analyses were carried out in order to identify the key reactions responsible for fuel consumption in the simulation targets.

Flame speed sensitivity analyses were performed using CHEMKIN-PRO's inbuilt utility [26], which calculates first-order sensitivity coefficients for the predicted mass flow rate, which corresponds to the flame speed.

Ignition delay time "brute force" sensitivity analyses were carried out by increasing and decreasing every reaction rate expression by a factor of two resulting in the effect on the predicted ignition delay time. The sensitivity coefficient is defined as:

$$S = \frac{\ln(\tau_+/\tau_-)}{\ln(k_+/k_-)} = \frac{\ln(\tau_+/\tau_-)}{\ln(2.0/0.5)}$$

where τ_+ corresponds to the ignition delay time calculated with the increased rate constant and vice versa. A positive sensitivity coefficient indicates an inhibiting reaction and vice versa.

3.5. Flux analyses

Flux analyses were carried out to determine the most important reactions responsible for fuel consumption and the further underlying pathways leading to final products at various temperature regimes. They were performed assuming a constant volume reactor and were taken at the time corresponding to 20% fuel consumption.

4. Computational method

4.1. Rate constant calculation

Rate constant calculations have been carried out for the important reactions associated with 1-butene oxidation. The M062X method [30] with the 6-311++G(d,p) basis set were used in the geometry optimizations and frequency calculations of all of the species involved in this reaction using Gaussian 09 [31]. The same method was used to determine the potential energy surface scans for the individual hindered rotors associated with reactant and transition state. The electronic single point energies have been calculated at CCSD(T)/cc-pvXZ level of theory (where $X = D$, T and Q) which were extrapolated to the complete basis set (CBS) limit [32,33].

Conventional transition-state theory [34] with an asymmetric Eckart tunneling correction [35] has been used to calculate the high-pressure limit rate constants in this work. The low-frequency torsional conserved modes were treated as hindered rotors.

For systems containing arbitrary numbers of wells and product/isomer channels, pressure dependent rate constants were calculated by using the ChemDis code [36,37], based on Quantum-Rice–Ramsperger–Kassel (QRRK) theory using a Modified Strong Collision (MSC) approximation for Collisional Energy Transfer (CET).

4.2. Thermochemistry calculation

The thermodynamic parameters for all of new species pertaining to the 1-butene sub-mechanism were calculated based on the group additivity method developed by Benson [38] with updated group values by Burke et al. [39] and utilizing the THERM program developed by Ritter and Bozzelli [40]. The thermodynamic parameters for all of the species involved in the 1-butene sub-mechanism in addition to the entire mechanism are provided as Supplementary material.

5. Chemical kinetic mechanism development

The current mechanism was developed based on a series of previous work studies, including:

- H_2/O_2 sub-mechanism developed by Kéromnès et al. [41].
- C_1–C_2 sub-mechanism (AramcoMech 1.3) developed by Metcalfe et al. [11].

Table 3
Arrhenius coefficients for the important reactions (cm^3/mol/s/cal units).

No.	Reactions	*A*	*n*	E_a	Reference
1	C_4H_8-1 + O_2 ↔ $\dot{C}_4H_7$1-3 + $H\dot{O}_2$	1.00E+14	0.00	37,190	[43]
2	C_4H_8-2 + O_2 ↔ $\dot{C}_4H_7$1-3 + $H\dot{O}_2$	2.00E+14	0.00	39,390	[43]
3	C_4H_8-1 + $\dot{O}H$ ↔ $\dot{C}_4H_7$1-3 + H_2O	1.01E+06	2.20	−437.2	[44]
4	C_4H_8-1 + $\dot{O}H$ ↔ $\dot{C}_4H_7$1-4 + H_2O	8.60E+06	2.03	2623.1	[44]
5	C_4H_8-1 + $\dot{O}H$ ↔ $\dot{C}_4H_7$1-2 + H_2O	3.00E+06	1.97	2847.7	[44]
6	C_4H_8-1 + $\dot{O}H$ ↔ p$\dot{C}_4H_8$OH-2	2.10E+06	1.81	−3292.3	[45,46]
7	C_4H_8-1 + $\dot{O}H$ ↔ s$\dot{C}_4H_8$OH-1	7.00E+05	1.80	−3290.2	[45,46]
8	C_4H_8-1 + $\dot{H}$ ↔ C_3H_6 + $\dot{C}H_3$ (DUP1)	1.32E+20	−1.46	15,383	[19]
9	C_4H_8-1 + $\dot{H}$ ↔ C_3H_6 + $\dot{C}H_3$ (DUP2)	1.00E+33	−5.49	31,922	[19]
10	$\dot{C}_4H_7$1-3 ↔ $\dot{C}_4H_7$1-4	5.62E−12	7.19	36,200.8	[19]
11	$\dot{C}_4H_7$1-4 ↔ C_2H_4 + $\dot{C}_2H_3$	2.84E+10	0.99	38,998.8	[19]
12	$\dot{C}_4H_7$1-3 + O_2 ↔ C_4H_6 + $H\dot{O}_2$	1.07E+00	3.71	9322	[47]
13	$\dot{C}_4H_7$1-3 + $H\dot{O}_2$ ↔ $C_4H_7$2-1OOH	2.80E+20	−2.96	−2503	[48]
14	$\dot{C}_4H_7$1-3 + $H\dot{O}_2$ ↔ $C_4H_7$1-3OOH	3.45E+19	−2.71	−3140	[48]
15	$\dot{C}_4H_7$1-3 + $H\dot{O}_2$ ↔ $C_4H_7\dot{O}$ + $\dot{O}H$	4.44E+42	−8.67	21,071	[48]
16	$\dot{C}_4H_7$1-3 + $H\dot{O}_2$ ↔ $C_4H_7\dot{O}$2-1 + $\dot{O}H$	2.18E+42	−8.58	21,090	[48]
17	$\dot{C}_4H_7$1-3 + $\dot{C}H_3$(+M) ↔ C_5H_{10}-2(+M)	1.00E+14	−0.32	−262.3	[49]
18	$\dot{C}_4H_7$1-3 + $\dot{C}H_3$(+M) ↔ cC_5H_{10}(+M)	1.00E+14	−0.32	−262.3	[49]
19	sQC_4H_7OHp-4 + O_2 ↔ sQC_4H_7OHp-4O_2	3.43E+16	−1.63	198.7	[50]
20	sQC_4H_8Op → C_2H_5CHO + CH_2O + $\dot{O}H$	5.36E+12	−0.08	10,790	[51]

- CH_4/DME sub-mechanism developed by Burke et al. [42].
- Propene/allene/propyne sub-mechanism developed by Burke et al. [16, 17].
- Isobutene sub-mechanism developed by Zhou et al. [18].
- 2-Butene sub-mechanism developed by Li et al. [19].

The current model has been developed and presented in our 2-butene study [19]. In this paper, the model will be validated, not only against the new experimental data presented in this study, but also against a large variety of experimental data and a number of other literature models, provided as Supplementary material. Key reactions for 1-butene oxidation at different temperatures and pressures have been highlighted using the "brute force" and flame speed sensitivity analyses and flux analyses, discussed in detail in the following sections. The 1-butene combustion chemistry model predicts well a variety of experimental data, including ignition delay times, speciation measurements as a function of time and/or temperature and height above the burner surface in addition to flame speed measurements. The comprehensive kinetic mechanism AramcoMech 2.0, thermochemistry, transport files and glossary are provided as Supplementary material and are available for download at http://c3.nuigalway.ie/mechanisms.html.

5.1. Important reaction classes highlighted

The important reactions for 1-butene ignition delay times in an RCM and/or a shock tube are highlighted by our "brute force" sensitivity analyses.

Figure 3 shows the sensitivity result comparison for the pressure of 10 and 30 atm, at $\varphi = 1.0$ in 'air' (21% O_2:79% N_2), $T = 1250$, 950 and 700 K, Fig. 4 shows the sensitivity result comparison for $\varphi = 0.5$, 1.0 and 2.0, at $p = 30$ atm, $T = 700$, 950 and 1250 K.

All of the reactions highlighted here will be discussed and explained in detail in the following sections and the major reaction pathways are shown in Fig. 5 and their associated Arrhenius coefficients are provided in Table 3.

5.2. Unimolecular decomposition

Speciation measurements of 1-butene pyrolysis in flow reactor [6] are sensitive to 1-butene decomposition. Four important reactions involving C–C and C–H bond breaking of 1-butene, which we described in the recombination direction, were included in this work:

- $\dot{C}_3H_5$-a + $\dot{C}H_3$ (+M) ↔ C_4H_8-1 (+M)
- $\dot{C}_2H_5$ + $\dot{C}_2H_3$ (+M) ↔ C_4H_8-1 (+M)
- $\dot{C}_4H_7$1-3 + $\dot{H}$ (+M) ↔ C_4H_8-1 (+M)
- $\dot{C}_4H_7$1-4 + $\dot{H}$ (+M) ↔ C_4H_8-1 (+M)

The pressure-dependent rate constants for the two C–C bond fission reactions were adapted from the study by Tsang et al. [49,52]. The allylic site C–H bond fission reaction was found to be the most favored channel, and the rate constant was estimated to best validate the 1-butene pyrolysis experiments presented by Zhang et al. [6].

5.3. Fuel–O_2 reactions

For H atom abstraction by molecular oxygen, only the reaction resulting in the formation of 1-methlyallyl ($\dot{C}_4H_7$1-3) and hydroperoxyl radicals was found to be sensitive, while abstractions from the other carbon atom sites were not competitive.

- C_4H_8-1 + O_2 ↔ $\dot{C}_4H_7$1-3 + $H\dot{O}_2$
- C_4H_8-2 + O_2 ↔ $\dot{C}_4H_7$1-3 + $H\dot{O}_2$

As shown in Figs. 3 and 4, at intermediate ($T = 950$ K) and high temperatures ($T = 1250$ K), H atom abstraction from the allylic carbon atom site on 1- and 2-butene results in the formation of the same products, but these two reactions have different effects in either promoting or inhibiting reactivity. This is because the chain branching reaction between 1-butene and molecular oxygen forms two radicals ($\dot{C}_4H_7$1-3 and $H\dot{O}_2$) promoting reactivity. Conversely, in the second reaction the thermodynamics results to the formation of the two stable molecules (C_4H_8-2 + O_2), thus inhibiting reactivity. In this way both the 1- and 2-butene oxidation mechanisms are intrinsically linked and a mechanism for one must contain the other.

The rate constants for these two abstraction reactions were determined based on the Evans–Polanyi relationship developed by Somers et al. [43], in which the activation energy was found to relate to the heat of reaction via:

$$E_a = 1.06 * \Delta_r H - 9.44$$

in kJ mol^{-1} units. The frequency factors were estimated based on a best fit to experimental data over a wide range of conditions from the jet-stirred reactor, pre-mixed flame and shock tube. Figure 6 shows the influence of this adjustment on IDT prediction.

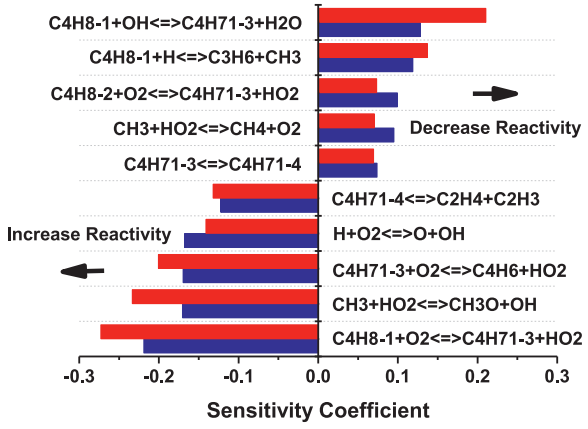

(a) $T = 1250$ K

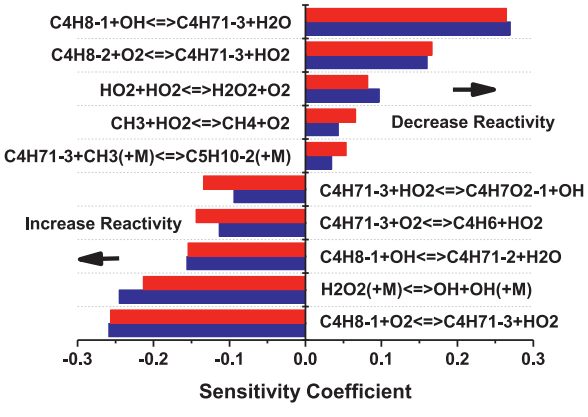

(b) $T = 950$ K

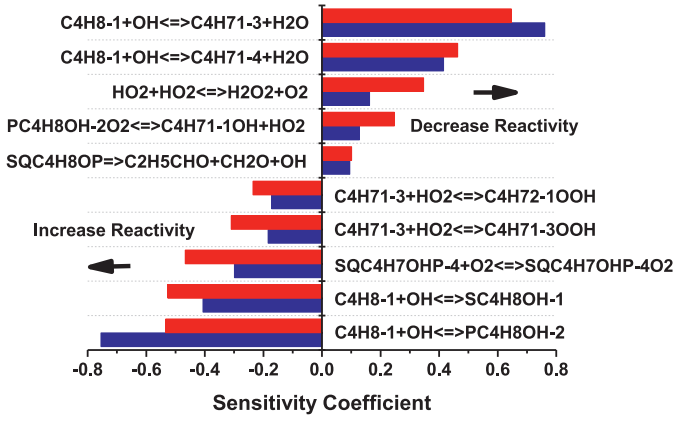

(c) $T = 700$ K

Fig. 3. Sensitivity analyses for 1-butene, $\phi = 1.0$ in 'air', $p =$ ■ 10 atm, ■ 30 atm.

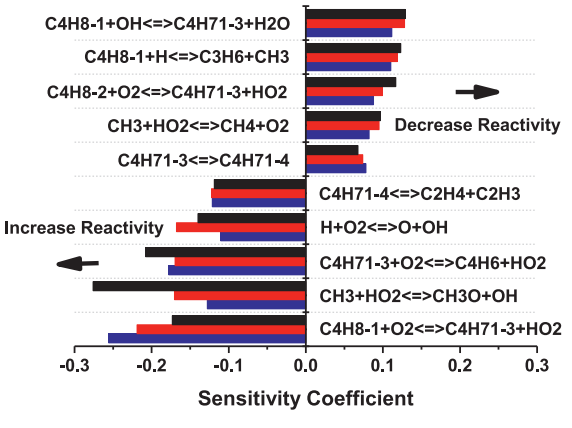

(a) $T = 1250$ K

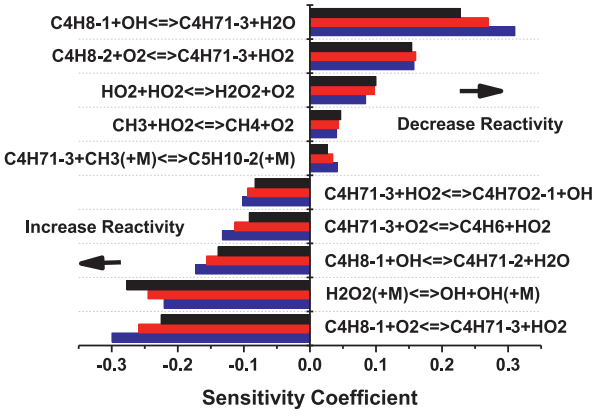

(b) $T = 950$ K

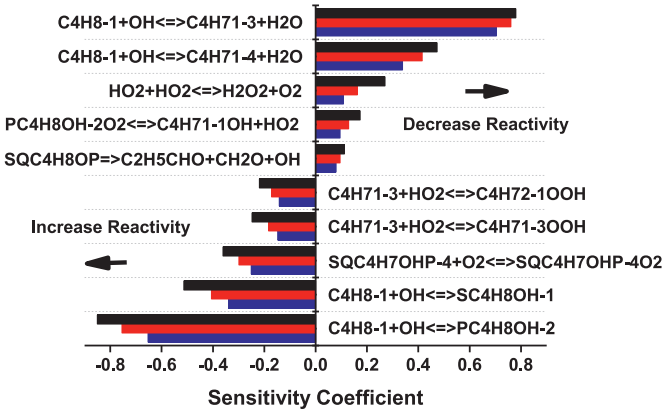

(c) $T = 700$ K

Fig. 4. Sensitivity analyses for 1-butene oxidation, $p = 30$ atm, $\phi =$ ■ 0.5, ■ 1.0 and ■ 2.0 in 'air'.

5.4. Fuel–radical reactions

H-atom abstraction reactions by various radicals from 1-butene have been included in this work. There are four different types of hydrogen atom (methyl site, secondary allylic C atom site, secondary vinylic C atom site and primary vinylic C atom site) on 1-butene as shown in Fig. 7.

Figure 7 shows the bond dissociation energies of 1-butene molecule. Due to the much lower bond dissociation energy (BDE) of the secondary allylic hydrogen atoms (85.5 kcal mol^{-1}) which are approximately 20 kcal mol^{-1} weaker than the other three types of C–H bonds in the molecule, abstraction of these H-atom and thus the formation of 1-methylallyl ($\dot{C}_4H_7$1-3) radicals is dominant.

5.4.1. C_4H_8-1 + $\dot{O}H$ ↔ products

The hydroxyl radical is extremely important in promoting reactivity in combustion processes. For the reaction of hydroxyl radical with 1-butene, both abstraction and addition pathways are included in the current kinetic mechanism

- $C_4H_8\text{-}1 + \dot{O}H \leftrightarrow \dot{C}_4H_7\text{1-4} + H_2O$
- $C_4H_8\text{-}1 + \dot{O}H \leftrightarrow \dot{C}_4H_7\text{1-3} + H_2O$
- $C_4H_8\text{-}1 + \dot{O}H \leftrightarrow \dot{C}_4H_7\text{1-2} + H_2O$

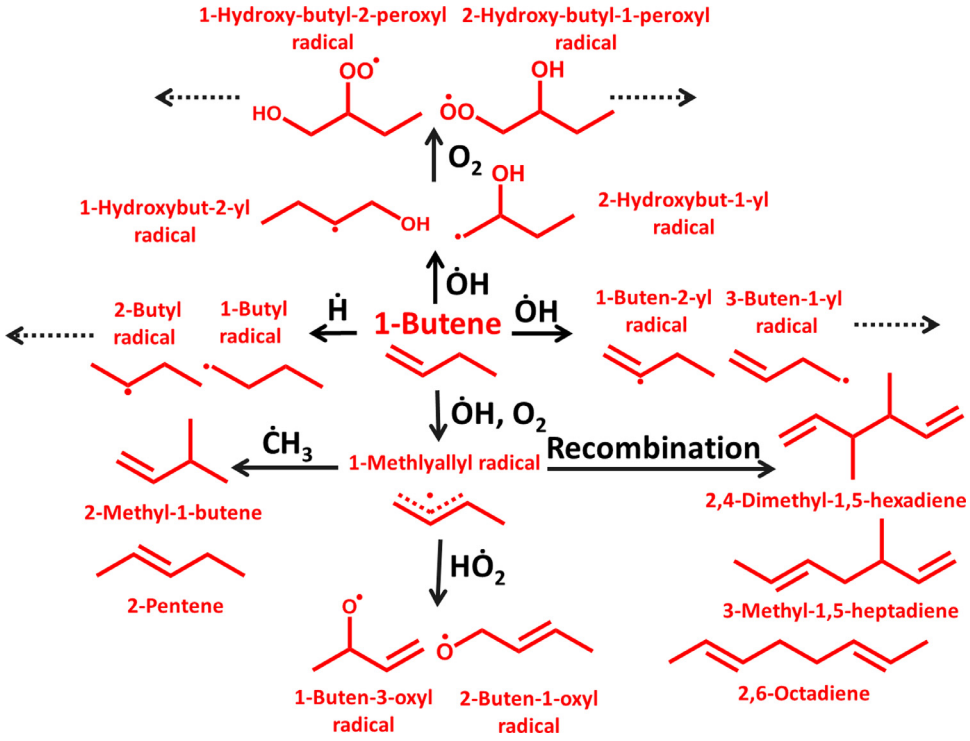

Fig. 5. Generalized reaction pathways included in this work for 1-butene oxidation.

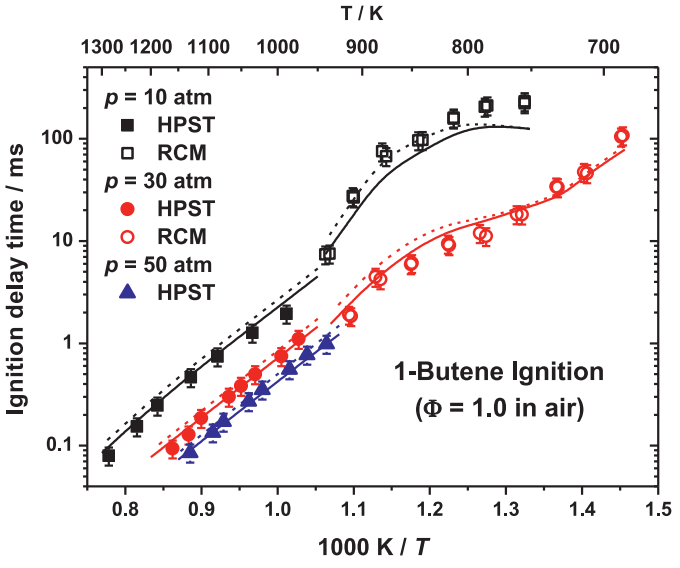

Fig. 6. Effect of changing the $C_4H_8\text{-}1 + O_2 \leftrightarrow \dot{C}_4H_7\text{1-3} + H\dot{O}_2$ rate constant on IDT at $\varphi = 1.0$ in air, $p = 10$, 30 and 50 atm. Solid line: this study, dashed line: A-factor × 0.5.

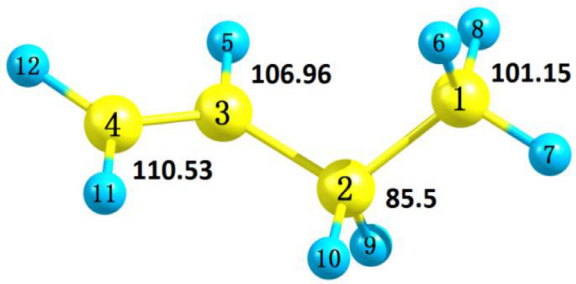

Fig. 7. 1-Butene structure and C–H bond dissociation energies (in kcal mol^{-1}), ● C atom, ● H atom.

- $C_4H_8\text{-}1 + \dot{O}H \leftrightarrow \dot{C}_4H_7\text{1-}1 + H_2O$.

As shown in Figs. 3 and 4, the reaction leading to the formation of 1-methylallyl radicals is the most inhibiting reactivity throughout the entire temperatures range. The rate constants for the $C_4H_8\text{-}1 + \dot{O}H$ abstraction reactions were adopted from the experimental and theoretical study of Vasu et al. [44] at the CCSD(T)/6-311++G(d,p)//QCISD/6-31G(d,p) level of theory, and it has been decreased by a factor of 2.6 which is the uncertainty provided by Vasu et al. in taking the contribution from the pathway for ȮH radical addition and the uncertainty in their experiments into consideration. Figure 8 shows a rate constant comparison for abstraction by ȮH radicals on different sites on 1-butene on a per H-atom basis.

It can be seen that abstraction from the allylic site is the fastest followed by primary carbon site, with vinylic site being the slowest, corresponding to the C–H bond dissociation energies. Figure 9 shows the rate constants comparison for the allylic radical formation reactions C_3H_6, iC_4H_8, $C_4H_8\text{-}1$ and $C_4H_8\text{-}2 + \dot{O}H$ (per H-atom basis). It can be seen that the rate constants for abstraction from the primary allylic sites on C_3H_6, iC_4H_8 and $C_4H_8\text{-}2$ are within 30% of one another at combustion temperatures (700–1500 K). Furthermore, the rate constant for abstraction from the secondary allylic site on 1-butene is faster compared to abstraction of a primary allylic H-atom, which is consistent with the differences in the C–H bond dissociation energies.

- $C_4H_8\text{-}1 + \dot{O}H \leftrightarrow p\dot{C}_4H_8OH\text{-}2$
- $C_4H_8\text{-}1 + \dot{O}H \leftrightarrow s\dot{C}_4H_8OH\text{-}1$

As shown in Figs. 3 and 4, ȮH radical addition to $C_4H_8\text{-}1$ is the most important reaction promoting reactivity at low temperatures ($T = 700$ K). This is because chain branching can subsequently occur via radical addition of the 1-butene + ȮH adduct to O_2, internal H-atom isomerization, a second addition to O_2, with the decomposition of the nascent ketohydroperoxide species ultimately promoting reactivity via the generation of ȮH radicals, as shown in Fig. 10. The rate constants for these reactions were estimated by analogy

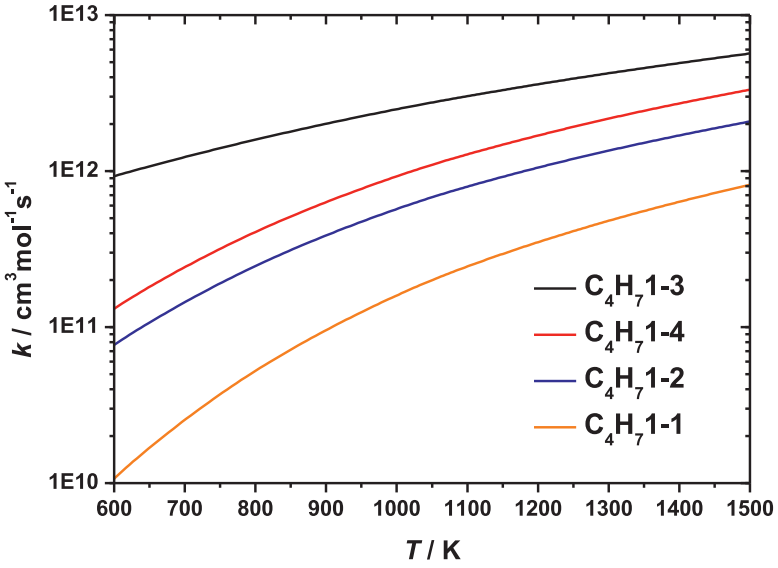

Fig. 8. Comparison of rate constants for C_4H_8-1 + ȮH at different sites on a per H-atom basis.

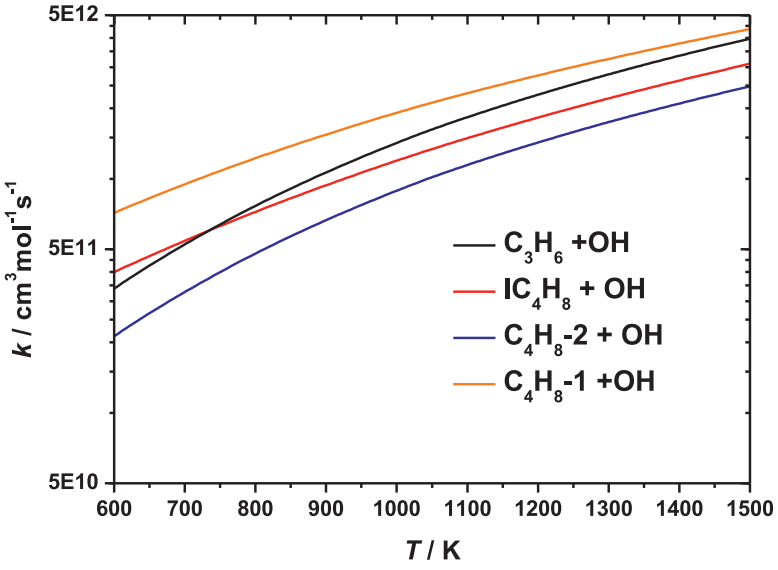

Fig. 9. Comparison of rate constants for abstraction of allylic H-atom by ȮH from C_3H_6, iC_4H_8, C_4H_8-2 and C_4H_8-1 + ȮH on a per H-atom basis.

with the propene/ȮH radical system as calculated by Zádor et al. [45]. Moreover, a branching ratio of 75:25 in favor of addition to the terminal carbon was adopted based on the experimental study by Loison et al. [46]. The influence of this branching ratio on the ignition delay times in the low temperature range can be seen in Fig. 11.

5.4.2. C_4H_8-1 + Ḣ ↔ products

- C_4H_8-1 + Ḣ ↔ $\dot{C}_4H_7$1-4 + H_2
- C_4H_8-1 + Ḣ ↔ $\dot{C}_4H_7$1-3 + H_2
- C_4H_8-1 + Ḣ ↔ $\dot{C}_4H_7$1-2 + H_2
- C_4H_8-1 + Ḣ ↔ $\dot{C}_4H_7$1-1 + H_2
- C_4H_8-1 + Ḣ ↔ p$\dot{C}_4H_9$
- C_4H_8-1 + Ḣ ↔ s$\dot{C}_4H_9$
- C_4H_8-1 + Ḣ ↔ C_2H_4 + $\dot{C}_2H_5$
- C_4H_8-1 + Ḣ ↔ C_3H_6 + $\dot{C}H_3$
- C_4H_8-1 + Ḣ ↔ C_4H_8-2 + Ḣ

As shown in Figs. 3 and 4, when Ḣ atom adds to the terminal carbon atom, the chemically activated reaction C_4H_8-1 + Ḣ ↔ C_3H_6 + $\dot{C}H_3$ becomes sensitive, inhibiting reactivity. This reaction results in the consumption of atomic hydrogen producing relatively unreactive methyl radicals. In the flame speed sensitivity analysis shown in Fig. 12, this reaction is the only sensitive fuel chemistry reaction, also inhibiting reactivity.

However, Ḣ-atom addition to the non-terminal carbon atom in 1-butene results in the formation of C_2H_4 + $\dot{C}_2H_5$, which ultimately generates two vinyl radicals and a hydrogen atom, promoting reactivity. The rate constants for this reaction class were calculated on the $\dot{C}_4H_9$ potential energy surface (PES) at the CCSD(T)/cc-pVXZ//M062X/6-311++G(d,p) level of theory (where X = D, T and Q) and extrapolated to the complete basis set (CBS) limit [32, 33].

5.4.3. C_4H_8-1 + $H\dot{O}_2$ ↔ products

Reactions that involve hydroperoxyl radicals are most influential at elevated pressures and lower temperatures. Under these conditions, the stabilization of Ḣ + O_2 (+M) ↔ $H\dot{O}_2$ (+M) is favored over the chain branching reaction H + O_2 ↔ Ö + ȮH.

H-abstraction reaction by $H\dot{O}_2$

- C_4H_8-1 + $H\dot{O}_2$ ↔ $\dot{C}_4H_7$1-4 + H_2O_2

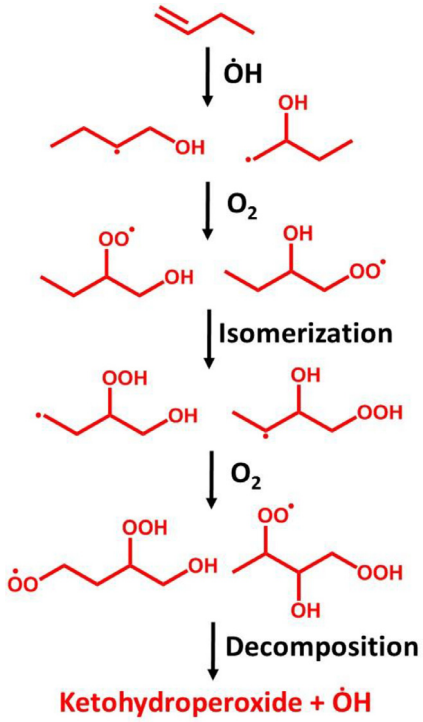

Fig. 10. Low temperature chain branching reaction pathways for 1-butene oxidation.

- $C_4H_8\text{-}1 + H\dot{O}_2 \leftrightarrow \dot{C}_4H_7\text{-}1\text{-}3 + H_2O_2$
- $C_4H_8\text{-}1 + H\dot{O}_2 \leftrightarrow \dot{C}_4H_7\text{-}1\text{-}2 + H_2O_2$
- $C_4H_8\text{-}1 + H\dot{O}_2 \leftrightarrow \dot{C}_4H_7\text{-}1\text{-}1 + H_2O_2$

The rate constants for abstraction reactions of 1-butene and hydroperoxyl radicals are adopted by analogy with the theoretical study on propene + $H\dot{O}_2$ from Zádor et al. [53].

$H\dot{O}_2$ addition to C_4H_8-1

- $C_4H_8\text{-}1 + H\dot{O}_2 \leftrightarrow \dot{C}_4H_8OOH1\text{-}2$
- $C_4H_8\text{-}1 + H\dot{O}_2 \leftrightarrow \dot{C}_4H_8OOH2\text{-}1$
- $C_4H_8\text{-}1 + H\dot{O}_2 \leftrightarrow \dot{C}_4H_8OOH2\text{-}3$
- $C_4H_8\text{-}1 + H\dot{O}_2 \leftrightarrow C_4H_8O1\text{-}2 + \dot{O}H$
- $C_4H_8\text{-}1 + H\dot{O}_2 \leftrightarrow C_4H_8O2\text{-}3 + \dot{O}H$
- $C_4H_8\text{-}1 + H\dot{O}_2 \leftrightarrow pC_4H_9\dot{O}_2$
- $C_4H_8\text{-}1 + H\dot{O}_2 \leftrightarrow sC_4H_9\dot{O}_2$
- $C_4H_8\text{-}1 + H\dot{O}_2 \leftrightarrow p\dot{C}_4H_9 + O_2$
- $C_4H_8\text{-}1 + H\dot{O}_2 \leftrightarrow s\dot{C}_4H_9 + O_2$
- $pC_4H_9\dot{O}_2 \leftrightarrow \dot{C}_4H_8OOH1\text{-}2$
- $pC_4H_9\dot{O}_2 \leftrightarrow \dot{C}_4H_8OOH1\text{-}3$
- $pC_4H_9\dot{O}_2 \leftrightarrow \dot{C}_4H_8OOH1\text{-}4$
- $sC_4H_9\dot{O}_2 \leftrightarrow \dot{C}_4H_8OOH2\text{-}1$
- $sC_4H_9\dot{O}_2 \leftrightarrow \dot{C}_4H_8OOH2\text{-}3$
- $sC_4H_9\dot{O}_2 \leftrightarrow \dot{C}_4H_8OOH2\text{-}4$
- $\dot{C}_4H_8OOH1\text{-}2 \leftrightarrow C_4H_8O1\text{-}2 + \dot{O}H$
- $\dot{C}_4H_8OOH1\text{-}3 \leftrightarrow C_4H_8O1\text{-}3 + \dot{O}H$
- $\dot{C}_4H_8OOH1\text{-}4 \leftrightarrow C_4H_8O1\text{-}4 + \dot{O}H$
- $\dot{C}_4H_8OOH2\text{-}4 \leftrightarrow C_4H_8O1\text{-}3 + \dot{O}H$
- $\dot{C}_4H_8OOH2\text{-}1 \leftrightarrow C_4H_8O1\text{-}2 + \dot{O}H$
- $\dot{C}_4H_8OOH2\text{-}3 \leftrightarrow C_4H_8O2\text{-}3 + \dot{O}H$
- $\dot{C}_4H_8OOH1\text{-}3 \rightarrow C_3H_6 + CH_2O + \dot{O}H$
- $\dot{C}_4H_8OOH2\text{-}4 \rightarrow C_2H_4 + CH_3CHO + \dot{O}H$

The rate constants for the addition reactions of hydroperoxyl radicals to 1-butene and the related reactions on the $C_4H_9O_2$ PES have been investigated by different groups [50,53–58]. Zádor et al. [53] calculated the rate constants for $H\dot{O}_2$ radical addition to the non-terminal unsaturated carbon atom in 1-butene to form a hydroperoxyl-alkyl radical and its following reaction to form a cyclic ether and a hydroxyl radical. The QCISD(T)/cc-pV∞Z//B3LYP/6-311++G(d,p) level of theory was used to obtain the electronic energy barrier heights. A MULTIWELL master equation analysis [59,60] was carried out based on these calculations resulting in pressure and temperature dependent rate constants. Villano et al. [54] presented high-pressure rate rules and branching ratios for the addition of $H\dot{O}_2$ to olefins through the concerted addition channel to form an alkylperoxyl radical ($H\dot{O}_2$ + olefin ↔ $\dot{R}O_2$) and through the radical addition channel to form a hydroperoxyl-alkyl radical ($H\dot{O}_2$ + olefin ↔ QOOH) at the CBS-QB3 level of theory combined with TST calculations. Pressure- and temperature-dependent rate constants were calculated for $H\dot{O}_2$ addition to the terminal site of 1-butene using an energy-grained master equation approach and QRRK calculations with a modified strong collision (MSC) approximation. Sharma et al. [55], Villano et al. [56,57], and Miyoshi et al. [50,58] carried out systematic investigations on the low-temperature chemistry reaction classes on the $C_4H_9O_2$ PES. Results from these studies were found to be in general good agreement.

Table 4
Recommended rate rules for H-atom abstraction from primary and secondary allylic sites on a per H-atom basis (cm^3/mol/s/cal units).

	Primary			Secondary		
	A	*n*	E_a	*A*	*n*	E_a
Ḣ	1.21E+05	2.46	4360	1.21E+03	3.05	2000
ȮH	7.33E+03	2.68	−827	5.05E+05	2.20	−437
$H\dot{O}_2$	4.87E−02	4.12	12,800	3.91E−01	3.97	11,700
O_2	5.90E+00	3.64	37,300	2.44E+01	3.48	34,800

5.4.4. C_4H_8-1 + $\dot{C}H_3$ ↔ products

Similar to H-atom abstraction by ȮH radicals described above, methyl radical can abstract a hydrogen atom from 1-butene from any of the four sites. However, only the channel producing 1-methylallyl radical and methane was found to be competitive. This reaction is predicted to be an important source of methane detected in the JSR. The recommendation in this study is an estimation taken from the recommendation of Tsang [49].

5.4.5. C_4H_8-1 + Ö ↔ products

Both abstraction and addition reactions of 1-butene with atomic oxygen did not show any significant sensitivity to any of the data sets presented in this study. Rate constants for abstraction reactions are adopted from the review by Tsang [49] while those for addition and taken by analogy with propene [16].

5.5. H-atom abstraction from the allylic site

In view of the importance of the above H-atom abstraction reactions from the secondary allylic site on 1-butene by various radicals and by molecular oxygen, and together with the consistent rate constants for primary allylic H-atom abstraction from propene [16,17], isobutene [18] and 2-butene [19] used in developing AramcoMech 2.0, a recommendation of rate rules for these important abstraction reactions are summarized in Table 4.

5.6. Allylic radical chemistry

The allylic radical is a resonantly-stabilized radical in each of the two resonance forms of which the unpaired electron is on an allylic carbon. As shown in Fig. 13, a 1-methylallyl radical can be formed by H atom abstraction from the secondary allylic carbon in 1-butene or the primary allylic carbon in 2-butene. This radical

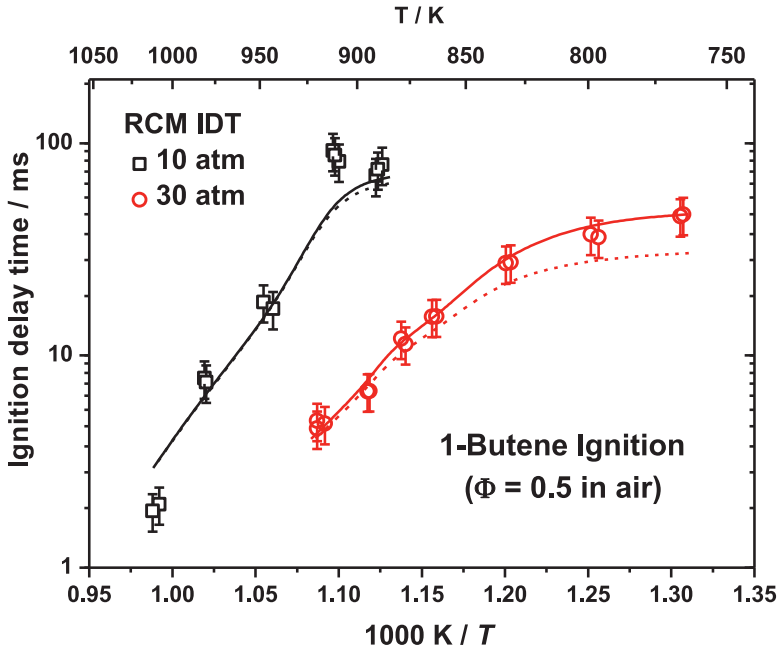

Fig. 11. Branching ratio effects from the ȮH terminal and central addition to C_4H_8-1 to ignition delay times at $\varphi = 0.5$, fuel in air, $p = 10$ and 30 atm. Terminal vs. central: solid line (75:25); dash line (50:50).

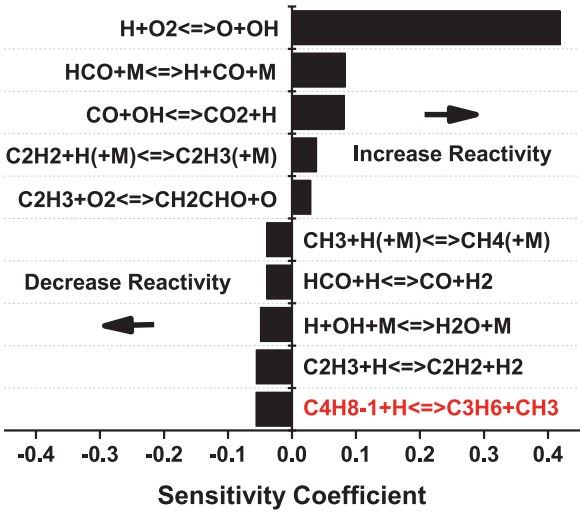

Fig. 12. Flame speed sensitivity analysis of C_4H_8-1/air laminar flame at $\varphi = 1.1$, $T_u = 298$ K, $p = 1$ atm.

Fig. 13. Stabilization of 1-methylallyl ($\dot{C}_4H_7$1-3) radical.

appears in all of the most sensitive reactions at all conditions of temperature and pressure presented in Figs. 3 and 4 as part of our sensitivity analyses.

5.6.1. Allylic radical reactions on C_4H_7 potential

- $\dot{C}_4H_7$1-3 ↔ $\dot{C}_4H_7$1-4
- $\dot{C}_4H_7$1-4 ↔ $C_2H_4 + \dot{C}_2H_3$
- $\dot{C}_4H_7$1-1 ↔ C_4H_6-1 + Ḣ
- $\dot{C}_4H_7$1-1 ↔ $C_2H_2 + \dot{C}_2H_5$
- $\dot{C}_4H_7$1-2 ↔ C_4H_6-1 + Ḣ
- $\dot{C}_4H_7$1-2 ↔ $C_4H_6$12 + Ḣ
- $\dot{C}_4H_7$1-2 ↔ C_3H_4-a + $\dot{C}H_3$
- $\dot{C}_4H_7$1-3 ↔ $C_4H_6$12 + Ḣ
- $\dot{C}_4H_7$1-3 ↔ C_4H_6 + Ḣ
- $\dot{C}_4H_7$1-4 ↔ C_4H_6 + Ḣ
- $\dot{C}_4H_7$2-2 ↔ C_4H_6-2 + Ḣ
- $\dot{C}_4H_7$2-2 ↔ $C_4H_6$12 + Ḣ
- $\dot{C}_4H_7$2-2 ↔ C_3H_4-p + $\dot{C}H_3$
- $\dot{C}_4H_7$1-3 ↔ $\dot{C}_4H_7$2-2

As shown in Figs. 3 and 4 at high temperatures ($T = 1250$ K), the isomerization of 1-methylallyl ($\dot{C}_4H_7$1-3) radical to 3-buten-1yl ($\dot{C}_4H_7$1-4) radical and vice versa, and the related β-scission reaction of 3-buten-1yl ($\dot{C}_4H_7$1-4) radical are sensitive reactions. The high-pressure limit rate constants for this reaction class were calculated on the C_4H_7 PES at CCSD(T)/cc-pvXZ//M062X/6-311++G(d,p) (where $X = D$, T and Q) level of theory, which have been discussed in Section 4.1.

5.6.2. Allylic radical reaction with O_2

- $\dot{C}_4H_7$1-3 + O_2 ↔ C_4H_6 + $H\dot{O}_2$

The reaction of 1-methylallyl ($\dot{C}_4H_7$1-3) radical with molecular oxygen promotes reactivity, as it consumes a stabilized allylic radical to generate a more reactive hydroperoxy radical. It is worth nothing that the reaction $\dot{C}_4H_7$1-3 + O_2 ↔ C_4H_6 + $H\dot{O}_2$ is not chemically activated via the sequence: $\dot{R} + O_2$ ↔ $R\dot{O}_2$ ↔ alkene + $H\dot{O}_2$, but is instead a direct abstraction. The well depth of the association reaction $\dot{C}_4H_7$1-3 + O_2 ↔ $C_4H_7$1-3$\dot{O}_2$ has been calculated here to be 19.9 kcal mol^{-1} using Gaussian 09 [31] and the composite CBS-QB3 method. The barrier for the subsequent concerted elimination of hydroperoxyl radical is 27.2 kcal mol^{-1} and so the reverse reaction to $\dot{C}_4H_7$1-3 + O_2 is kinetically favored over the formation of C_4H_6 + $H\dot{O}_2$. Alternatively, the formation of C_4H_6 + $H\dot{O}_2$ via a direct H-atom abstraction from the primary carbon side is possible, and the rate constant is adopted from the theoretical work of DeSain et al. [47].

5.6.3. Allylic radical reactions with $\dot{C}H_3$ radical

- $\dot{C}_4H_7$1-3 + $\dot{C}H_3$ (+M) ↔ C_5H_{10}-2 (+M)

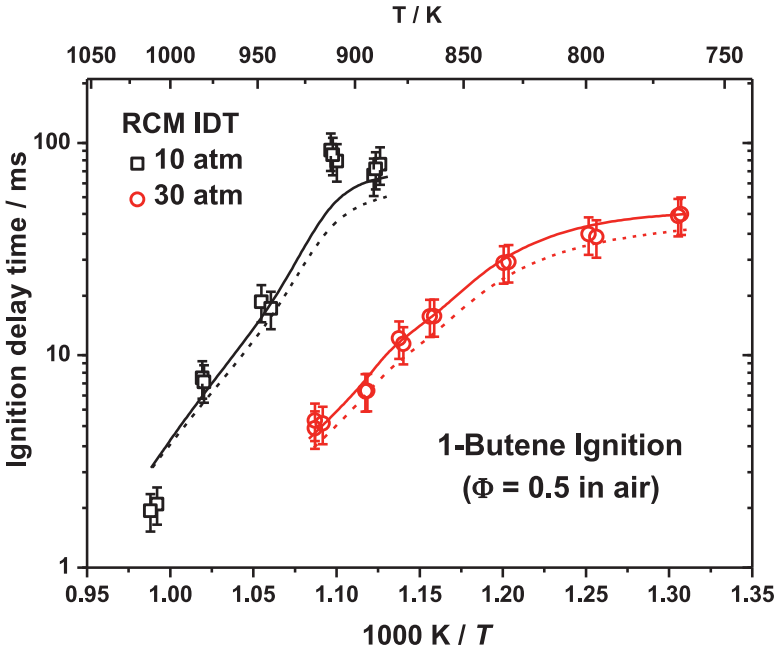

Fig. 14. Influence of rate constants for $\dot{C}_4H_7$1-3 + $\dot{C}_4H_7$1-3 to ignition delay times at $\varphi = 0.5$ in 'air', $p = 10$ and 30. Solid line: this study; dash line: excluding recombination channel.

- $\dot{C}_4H_7$1-3 + $\dot{C}H_3$ (+M) ↔ cC_5H_{10} (+M)

As shown in Figs. 3 and 4, at intermediate temperatures ($T = 950$ K), chain terminating reactions with methyl radicals resulting in the formation of 2-pentene (C_5H_{10}-2) and 3-methyl-1-butene (CC_5H_{10}) inhibit the reactivity of the system. Rate constants for these reactions are taken from Tsang [49] by analogy with allyl plus methyl radical recombination and adopting a branching ratio of 50:50 based on the spin densities of carbon atoms calculated with the M062X method [30] and the 6-311++G(d,p) basis set.

5.6.4. Allylic radical self-recombination

- $\dot{C}_4H_7$1-3 + $\dot{C}_4H_7$1-3 ↔ C_8H_{14}1-5,3-4
- $\dot{C}_4H_7$1-3 + $\dot{C}_4H_7$1-3 ↔ C_8H_{14}1-5,3
- $\dot{C}_4H_7$1-3 + $\dot{C}_4H_7$1-3 ↔ C_8H_{14}2-6

1-methylallyl ($\dot{C}_4H_7$1-3) radical can also undergo self-recombination to form 2,6-octadiene, 3-methyl,1-5-heptadiene and 3,4-dimethyl,1-5-hexadiene, and we adopted a branching ratio of 1:2:1 as explained in Section 5.6.3. These chain terminating reactions inhibit reactivity at low and intermediate temperatures. 1-methlyallyl radical self-reaction can also result in the formation of two alkene products. However, this reaction channel can be neglected as the rate constant is about two orders of magnitude lower than the self-recombination rate constants and does not contribute to fuel reactivity. The rate constants for this reaction class were taken by analogy with the allyl radical self-recombination study from Tranter and co-workers [61]. The influence of this reaction class to ignition delay time prediction is shown in Fig. 14.

5.6.5. Allylic radical reactions with $H\dot{O}_2$ radical

- $\dot{C}_4H_7$1-3 + $H\dot{O}_2$ ↔ $C_4H_7$1-3OOH
- $\dot{C}_4H_7$1-3 + $H\dot{O}_2$ ↔ $C_4H_7$1-$\dot{O}$ + $\dot{O}H$
- $\dot{C}_4H_7$1-3 + $H\dot{O}_2$ ↔ $C_2H_3COCH_3$ + H_2O
- $C_4H_7$1-3OOH ↔ $C_4H_7$1-$\dot{O}$ + $\dot{O}H$
- $C_4H_7$1-3OOH ↔ $C_2H_3COCH_3$ + H_2O
- $\dot{C}_4H_7$1-3 + $H\dot{O}_2$ ↔ $C_4H_7$2-1OOH
- $\dot{C}_4H_7$1-3 + $H\dot{O}_2$ ↔ $C_4H_7\dot{O}$2-1 + $\dot{O}H$
- $\dot{C}_4H_7$1-3 + $H\dot{O}_2$ ↔ sC_3H_5CHO + H_2O
- $C_4H_7$2-1OOH ↔ $C_4H_7\dot{O}$2-1 + $\dot{O}H$
- $C_4H_7$2-1OOH ↔ sC_3H_5CHO + H_2O

Unlike saturated alkanes in which the fuel molecule radical ($\dot{R}$) adds to molecular oxygen to form an $R\dot{O}_2$ radical with a stabilization energy of ~35 kcal mol^{-1}, the well depth for the reaction of $\dot{C}_4H_7$1-3 radicals with O_2 producing $C_4H_7$1-3$\dot{O}_2$ radicals has been calculated here (CBS-QB3) to be 19.9 kcal mol^{-1}. Thus, the back dissociation to $\dot{C}_4H_7$1-3 + O_2 is favored over the higher barrier isomerization or concerted elimination reaction processes. Instead, the reactions of 1-methylallyl and hydroperoxyl radicals are observed to be very important across a range of conditions, especially at low-to-intermediate temperatures, Figs. 3 and 4. The high-pressure limit rate constants of this reaction class were taken by analogy with the reaction of allyl radicals with hydroperoxyl radicals studied by Goldsmith et al. [48]. A branching ratio of 1:1 based on the spin densities of carbon atoms calculated with the M062X method [30] and the 6-311++G(d,p) basis set was adopted. Pressure dependent rate constants were calculated using QRRK/MSC theory.

5.7. Vinylic radical chemistry

- $\dot{C}_4H_7$1-2 + O_2 ↔ $C_4H_7$1-2$\dot{O}_2$
- $C_4H_7$1-2$\dot{O}_2$ ↔ $C_4H_7\dot{O}$1-2 + $\ddot{O}$
- $C_4H_7\dot{O}$1-2 ↔ CH_2CO + $\dot{C}_2H_5$
- $\dot{C}_4H_7$1-1 + O_2 ↔ $C_4H_7$1-1$\dot{O}_2$
- $C_4H_7$1-1$\dot{O}_2$ ↔ $C_4H_7\dot{O}$1-1 + $\ddot{O}$
- $C_4H_7$1-1$\dot{O}_2$ ↔ C_2H_5CHCO + $\dot{O}H$
- $C_4H_7\dot{O}$1-1 ↔ C_2H_3CHO + $\dot{C}H_3$

Vinylic radicals react with molecular oxygen to generate alkenylperoxy radicals ($C_4H_7$1-2$\dot{O}_2$ and $C_4H_7$1-1$\dot{O}_2$), followed by O–O bond fission resulting in the formation of $\ddot{O}$ atoms, which pronouncedly promote reactivity. To the best of our knowledge there have been no previous studies of the reactions of 1-buten-2-yl ($\dot{C}_4H_7$1-2) radical and 1-buten-1-yl ($\dot{C}_4H_7$1-1) radical with molecular oxygen. During recent studies of ethylene [11,62,63] and propene [16,17] combustion, it was found that the vinyl ($\dot{C}_2H_3$) radical, 2-propenyl ($\dot{C}_3H_5$-t) radical and 1-propenyl ($\dot{C}_3H_5$-s) radical

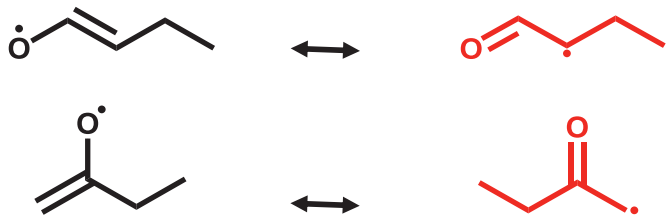

Fig. 15. Stabilization of $C_4H_7\dot{O}$1-1 and $C_4H_7\dot{O}$1-2 radicals.

were consumed almost entirely by reactions with molecular oxygen. The total rate constants for the reactions of both 1-buten-2-yl ($\dot{C}_4H_7$1-2) radical and 1-buten-1-yl ($\dot{C}_4H_7$1-1) radical with molecular oxygen and the subsequent O–O bond fission reactions recommended in this study are estimated by analogy to the reaction of vinyl radical with molecular oxygen from the high-level *ab initio* study by Goldsmith et al. [64]. The rate constants for the decomposition of the aldehyde and ketone radicals ($C_4H_7\dot{O}$1-1 and $C_4H_7\dot{O}$1-2) formed were calculated here at the CCSD(T)/CBS//M062X/6-311++G(d,p) level of theory. Note that, based on the geometry optimization and C–C bond scan calculations, the C=C–Ȯ structure in both $C_4H_7\dot{O}$1-1 and $C_4H_7\dot{O}$1-2 radicals stabilize to the Ċ–C=O structure, as shown in Fig. 15. Therefore, the β-scission of these two molecules will form $C_2H_3CHO + \dot{C}H_3$ and $CH_2CO + \dot{C}_2H_5$, respectively.

5.8. Alcohol radical chemistry

- $p\dot{C}_4H_8OH\text{-}2 + O_2 \leftrightarrow pC_4H_8OH\text{-}2\dot{O}_2$
- $s\dot{C}_4H_8OH\text{-}1 + O_2 \leftrightarrow sC_4H_8OH\text{-}1\dot{O}_2$

Alcohol radical chemistry forms a part of alkene oxidation as alcohol radicals ($p\dot{C}_4H_8OH$-2 and $s\dot{C}_4H_8OH$-1), formed by the addition of hydroxyl radicals to alkene fuels reactions are the most promoting reactions at low temperatures, Figs. 3 and 4. In a recent experimental and kinetic modeling study of the oxidation of the butanol isomers Sarathy et al. [65] presented detailed elementary reaction classes for the oxidation of these alcohol fuels It was also shown that the reaction of hydroxybutyl radicals with O_2 was and an important reaction class in controlling the reactivity of the system at low temperature, as this reaction is the first step in the low-temperature chain branching and propagation process.

- $pC_4H_8OH\text{-}2\dot{O}_2 \leftrightarrow sQC_4H_8\dot{O}p$
- $sQC_4H_8\dot{O}p \rightarrow C_2H_5CHO + CH_2O + \dot{O}H$
- $sC_4H_8OH\text{-}1\dot{O}_2 \leftrightarrow pQC_4H_8\dot{O}s$
- $pQC_4H_8\dot{O}s \leftrightarrow C_2H_5CHO + CH_2O + \dot{O}H$

The hydroxyalkyl peroxy radical ($R\dot{O}_2$) so generated can undergo Waddington-type reaction pathways [66,67], which have been included in the model. These reaction pathways involve the beta-$R\dot{O}_2$ radical undergoing a six-membered ring isomerization to abstract a hydrogen atom from the hydroxyl moiety (i.e. alkylhydroperoxide alkoxy radical), followed by a rapid decomposition to generate two aldehydes and an ȮH radical. For the $p\dot{C}_4H_8OH$-2 and $s\dot{C}_4H_8OH$-1 radicals this pathway leads to the formation of propanal, formaldehyde, and an ȮH radical. These reactions are chain propagating and compete directly with the alkyl type low-temperature chain branching pathways, thereby inhibiting reactivity. The rate constants for this reaction class were estimated by analogy with the theoretical work on 2-hydroxy-1,1-dimethylethyl ($i\dot{C}_4H_8OH$-it) and 2-hydroxy-2-methylpropyl ($i\dot{C}_4H_8OH$-ti) radicals addition to O_2 from Sun et al. [51]

- $R\dot{O}O \leftrightarrow QOOH$
- $R\dot{O}O \leftrightarrow enol + H\dot{O}_2$
- $QOOH \leftrightarrow cyclic\ ether + \dot{O}H$
- $QOOH + O_2 \leftrightarrow \dot{O}_2QOOH$
- $\dot{O}_2QOOH \leftrightarrow carbonyl\text{-}hydroperoxide + \dot{O}H.$

The low-temperature branching pathways promote reactivity with the rate constants for the intra-molecular H-abstraction of hydroxyalkyl peroxy radicals ($R\dot{O}_2$) to form hydroxyalkyl hydroperoxide (QOOH) radicals are adopted from the calculations of Sharma et al. [55]. The rate constants for the subsequent formation of a cyclic ether were adopted from the calculations of Villano et al. [56], while the rate constants for the second addition to molecular oxygen and the subsequent decomposition were adopted from the theoretical study of Miyoshi et al. [50].

6. Model validation

Figures 16 and 17 show model simulations compared with the experimental data for all mixtures. The overall uncertainty for each individual ignition delay time was estimated to be 20%, which are represented with *y*-axis error bars. Uncertainties in pressure, temperature, mixture composition, and those associated with the determination of the ignition delay time from the measured traces all contribute to the overall uncertainty. In these figures, solid symbols represent the experimental data obtained in the HPST and open symbols that recorded in the RCM with solid lines corresponding to IDTs calculated via constant-volume simulations, while dashed lines represent IDTs calculated using effective volume–time histories from the RCM to account for heat loss effects. For the IDTs simulations versus the experimental data recorded by Pan et al. [2] the non-ideal facility effect ($dp/dt = 4\%$) is included. In addition, the model has also been validated against the literature data listed in Table 1, and these results are presented as Supplementary material.

6.1. Influence of pressure on ignition delay time

Figure 16 shows the effect of pressure on ignition times obtained in both the HPST and in the RCM for fuel/air mixtures at $\varphi = 0.5$, 1.0 and 2.0. The experimental results show that reactivity increases with increasing pressure at all equivalence ratios. As the pressure increases so does the absolute concentration of reactants, resulting in the observed increase in reactivity. The mechanism is able to predict this effect over a wide range of pressures, temperatures and equivalence ratios.

6.2. Influence of equivalence ratio on ignition delay time

Ignition delay times were measured for fuel/air mixtures at equivalence ratios of 0.5, 1.0 and 2.0 at 10, 30 and 50 atm, Fig. 17. Again, the model is in good agreement across the entire temperature and pressure ranges.

In the range of low temperature conditions studied here, fuel-rich mixtures are fastest to ignite while fuel-lean mixtures being slowest. This is due to an increased concentration of fuel, as the chemistry based on the 1-butanol-2-yl ($p\dot{C}_4H_8OH$-2) radicals and 2-butanol-1-yl ($s\dot{C}_4H_8OH$-1) radicals, which are generated from the addition of hydroxyl radical to the C=C double bond, dominates reactivity, as discussed in Section 6.1 above.

However, at high temperatures, the difference in IDTs between three mixtures is much smaller, and based on the relative slopes of the data all datasets would appear to converge with the increasing temperature. This is due to the increasing importance of the chain branching reaction $\dot{H} + O_2 \leftrightarrow \ddot{O} + \dot{O}H$ at higher temperatures.

6.3. Flux analyses

Flux analyses were carried out at the same conditions as those presented in the sensitivity analyses, namely at $\varphi = 1.0$ in 'air' (21%

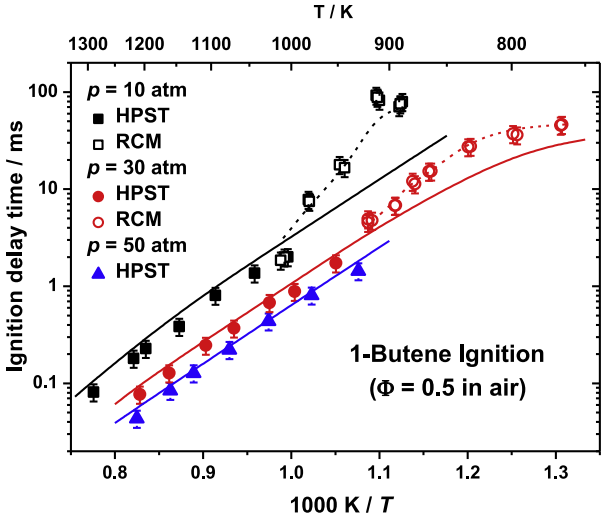

(a)

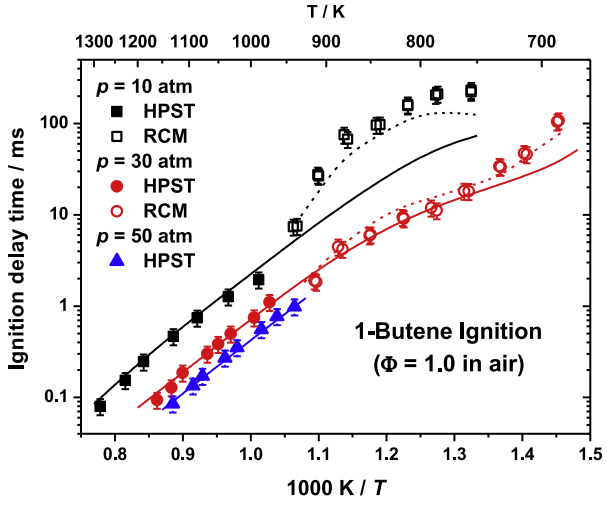

(b)

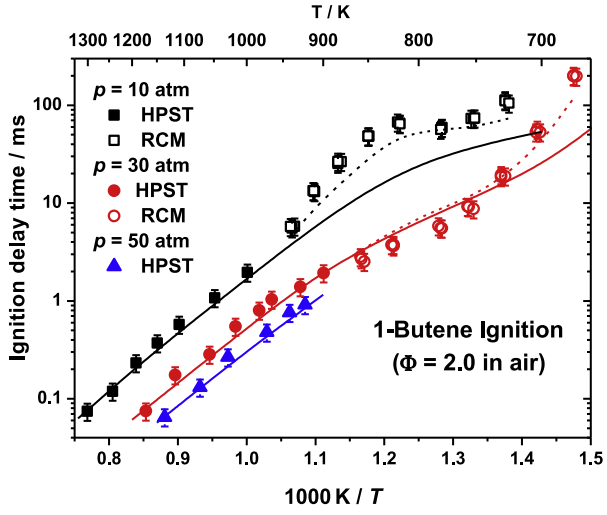

(c)

Fig. 16. Influence of pressure on 1-butene IDTs. (a) $\varphi = 0.5$, (b) $\varphi = 1.0$, (c) $\varphi = 2.0$. Solid lines are constant volume simulations, dashed lines include facility effects in the RCM experiments.

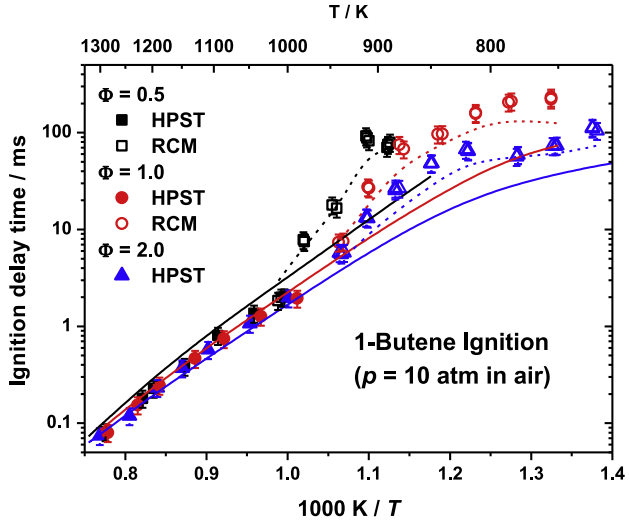

(a)

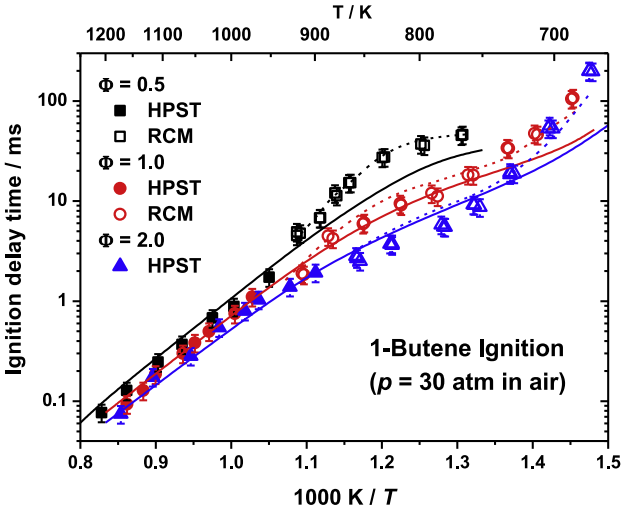

(b)

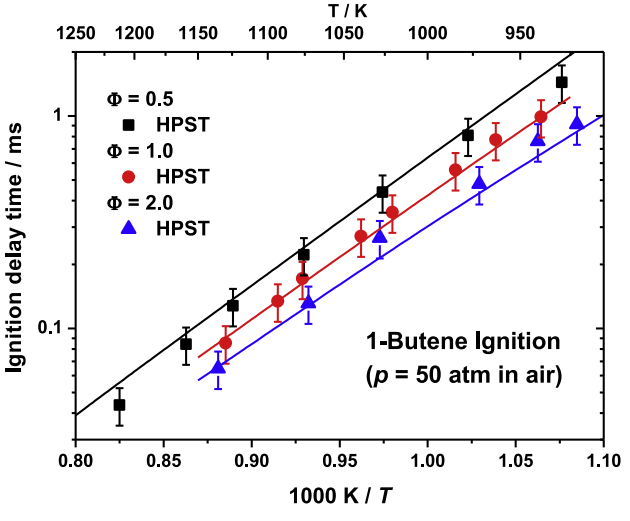

(c)

Fig. 17. Influence of equivalence ratio on 1-butene IDTs. (a) $p = 10$ atm, (b) $p = 30$ atm, (c) $p = 50$ atm. Solid lines are constant volume simulations, dashed lines include facility effects in the RCM experiments.

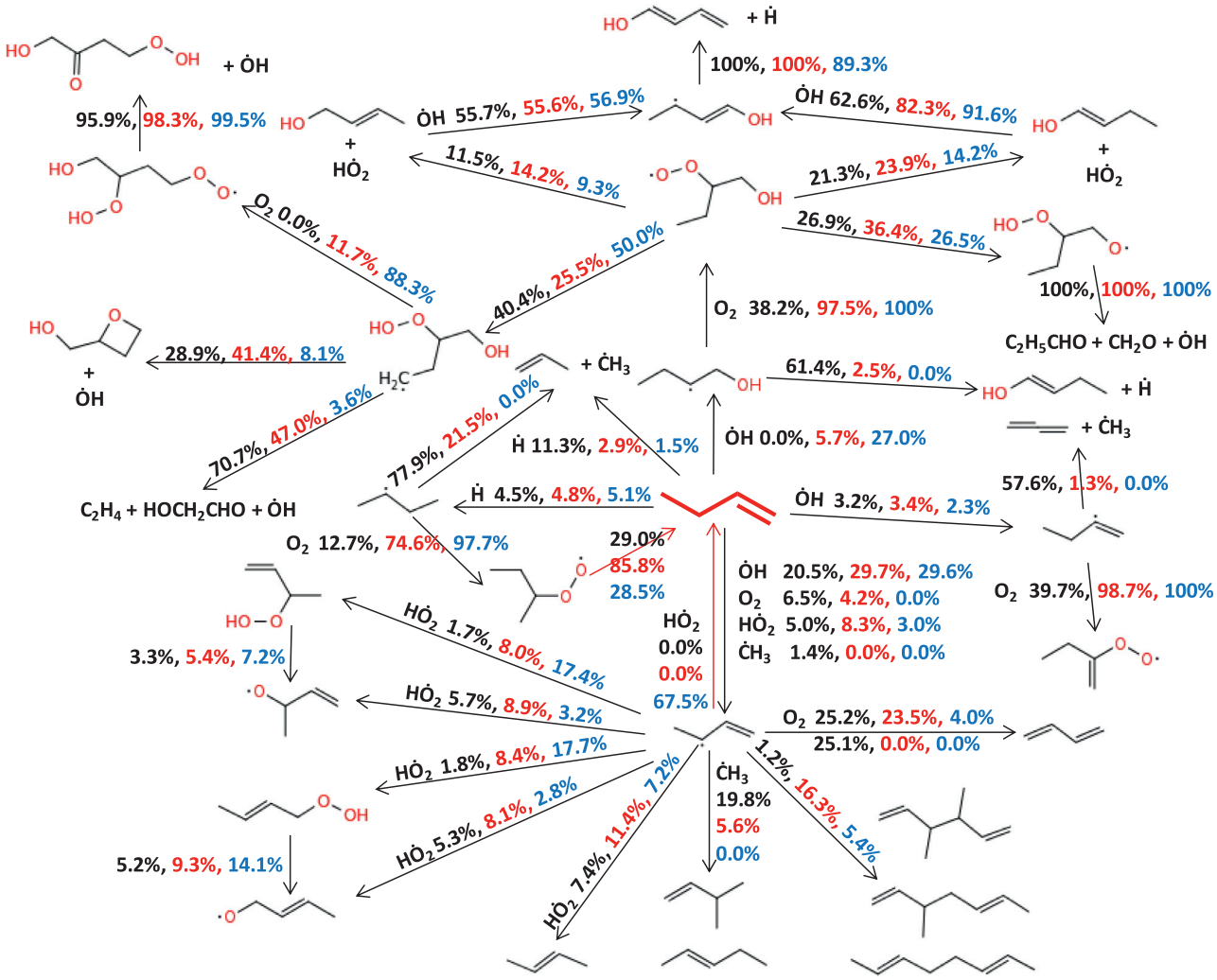

Fig. 18. Flux analysis for 1-butene oxidation at $\varphi = 1.0$, 30 atm and 20% fuel consumption. Black numbers: 1250 K; red numbers: 950 K; blue numbers: 700 K. (For interpretation of the references to color in this figure legend, the reader is referred to the web version of this article).

O_2: 79% N_2), $p = 30$ atm, $T = 700$ K, 950 K and 1250 K and at 20% fuel consumed (Fig. 18). These analyses cover the important reactions occurring at the various temperature regimes, particularly, for H-atom abstraction from the vinylic carbon site, only secondary vinylic H atom abstraction is shown here, and for the ȮH radical addition to the C=C double bond, only terminal carbon site addition is selected as a representative.

Initially the fuel is mainly consumed via H-atom abstraction by ȮH radicals across the entire temperature regime. Particularly at high temperature ($T = 1250$ K), Ḣ atoms can add to the C=C double bond to form propene and a methyl radical which contributes about 5% to overall fuel consumption. At intermediate temperatures ($T = 950$ K), H-atom abstraction from the vinylic carbon sites followed by the molecular oxygen addition and O–O bond fission consumes about 3.4% of the fuel, and this reaction pathway promotes the reactivity as discussed previously. At low temperatures ($T = 700$ K), the fuel is mainly consumed by the ȮH radical addition to the C=C double bond.

The allylic $\dot{C}_4H_7$1-3 radical is formed in most abundance and at high temperatures ($T = 1250$ K), it is mainly consumed via two pathways: (1) a uni-molecular decomposition to form 1,3-butadiene and a Ḣ atom; (2) a bi-molecular reaction with methyl radical to form either 2-pentene or 3-methyl-1-butene. The first reaction pathway promotes the reactivity, as it transfers a stabilized allylic radical into a very reactive Ḣ atom, which can undergo the typical chain branching reaction $\dot{H} + O_2 \leftrightarrow \ddot{O} + \dot{O}H$. The second reaction pathway is a chain terminating reaction which inhibits reactivity. At intermediate temperature ($T = 950$ K), $\dot{C}_4H_7$1-3 radicals are mainly consumed by two reaction pathways: (1) H-atom abstraction by molecular oxygen to form 1,3-butadiene and hydroperoxy radical; (2) self-recombination to form C_8 dienes. Again, these two reaction pathways promote and inhibit reactivity respectively as discussed in Sections 5.6.1 and 5.6.2. At low temperatures ($T = 700$ K), $\dot{C}_4H_7$1-3 radicals are mainly consumed by the addition and chemically activated reactions with $H\dot{O}_2$ radicals.

As to the alcohol radical ($p\dot{C}_4H_8OH$-2) consumption, at high temperature ($T = 1250$ K), they are mainly consumed by C–H bond β-scission to form an enol ($C_4H_7$1-1OH) and a Ḣ atom. At low and intermediate temperatures ($T = 700$ and 950 K), $p\dot{C}_4H_8OH$-2 radicals are mainly consumed by two reaction pathways: (1) Waddington type reaction pathways; (2) alkyl type low-temperature reaction pathways.

7. Conclusions

This work represents the first ignition delay study of 1-butene oxidation at elevated pressures in a HPST and in a RCM over a wide range of pressures, temperatures and equivalence ratios. The

results presented greatly expand the ignition delay time database available for mechanism validation for 1-butene oxidation.

It was found that an increase in reflected shock pressure resulted in shorter ignition delay times (higher reactivity) for all equivalence ratios investigated, which is typical of the influence of pressure on fuel reactivity. The effect of equivalence ratio on ignition delay times depended on the temperature of the experiment, where all mixtures had similar reactivity at higher temperatures and fuel-rich mixtures were most reactive at lower temperatures.

A detailed chemical kinetic mechanism has been developed to describe the combustion of 1-butene. It includes comprehensive low- and high temperature reaction pathways specific to unsaturated fuel molecules. Important reactions were identified through sensitivity and flux analyses. Rate constants have been adopted from experimental and theoretical studies where possible. However, for reactions where the literature is lacking, rate constants were calculated from *ab initio* methods or estimated. The mechanism is validated against our new experiments and relevant literature data. The current mechanism captures well most of the experimental results of ignition delay times, as well as flame speeds [9], species profiles from a JSR [4], a premixed flame [7] and a flow reactor [6].

From a kinetic point of view, it is found that H-atom abstraction from 1-butene by hydroxyl radicals significantly inhibits reactivity through the entire temperature range, as this reaction consumes very reactive hydroxyl radical to produce relatively unreactive stabilized 1-methyallyl ($\dot{C}_4H_7$1-3) radical. So the reactivity of 1-butene largely relies on the oxidation chemistry of this allylic radical, at high temperatures, it is mainly involved in the reactions on C_4H_7 potential and direct H-atom abstraction by molecular oxygen, and at intermediate and low temperatures, it is mainly involved in the bimolecular reactions with methyl and hydroperoxyl radicals. In addition, H-atom abstraction reactions from the other three different types of hydrogen atom (methyl site, primary and secondary vinylic C atom site) also show the importance at different temperature range, with methyl site H-atom abstraction inhibiting the reactivity at low temperature and vinylic site H-atom abstraction promoting the reactivity at intermediate temperature.

Together with the 2-butene study by Li et al. [19], it is also worth noting that, in 1-butene oxidation system, H-atom abstraction by molecular oxygen from allylic H-atom site in 1-butene and 2-butene promotes and inhibits reactivity respectively, and vice versa in 2-butene oxidation system. This is because the chain branching reaction between 1-butene and molecular oxygen forms two radicals, which ultimately promotes the reactivity, however the thermochemistry drives $\dot{C}_4H_7$1-3 and $H\dot{O}_2$ radicals results in the formation of two stable species: 2-butene and molecular oxygen, this chain terminating reaction inhibits the reactivity. Thus both the 1- and 2-butene oxidation mechanisms are intrinsically linked and need to be considered simultaneously.

As to the future research efforts, theoreticians and experimentalists are motivated to: a) accurately determine the low-temperature kinetic (rate constants and thermodynamic properties) of 1-methylallyl and *n*-butanol radicals and b) develop the rate rules of the important reaction classes for larger unsaturated hydrocarbons.

Acknowledgments

The authors thank the entire group members at Combustion Chemistry Centre for helpful discussions. This work at NUI Galway was supported by Saudi Aramco under the FUELCOM program.

Supplementary materials

Supplementary material associated with this article can be found, in the online version, at doi:10.1016/j.combustflame.2017.03.023.

References

[1] G.E.H. James H. Gary, MarkJ. Kaiser, Petroleum refining: technology and economics, CRC Press, 2007.
[2] L. Pan, E. Hu, J. Zhang, Z. Tian, X. Li, Z. Huang, A high pressure shock tube study of 1-butene oxidation and its comparison with n-butane and alkenes, Fuel 157 (2015) 21–27.
[3] B. Heyberger, N. Belmekki, V. Conraud, P.-A. Glaude, R. Fournet, F. Battin-Leclerc, Oxidation of small alkenes at high temperature, Int. J. Chem. Kinet. 34 (2002) 666–677.
[4] Y. Fenard, G. Dayma, F. Halter, F. Foucher, Z. Serinyel, P. Dagaut, Experimental and modeling study of the oxidation of 1-butene and cis-2-butene in a jet–stirred reactor and a combustion vessel, Energy Fuels 29 (2015) 1107–1118.
[5] A. Chakir, M. Cathonnet, J.C. Boettner, F. Gaillard, Kinetic study of 1-butene oxidation in a jet-stirred flow reactor, Symp. (Int.) Combust. 22 (1989) 873–881.
[6] Y. Zhang, J. Cai, L. Zhao, J. Yang, H. Jin, Z. Cheng, Y. Li, L. Zhang, F. Qi, An experimental and kinetic modeling study of three butene isomers pyrolysis at low pressure, Combust. Flame 159 (2012) 905–917.
[7] M. Schenk, L. Leon, K. Moshammer, P. Oßwald, T. Zeuch, L. Seidel, F. Mauss, K. Kohse-Höinghaus, Detailed mass spectrometric and modeling study of isomeric butene flames, Combust. Flame 160 (2013) 487–503.
[8] S.G. Davis, C.K. Law, Determination of and fuel structure effects on laminar flame speeds of C1 to C8 hydrocarbons, Combust. Sci. Technol. 140 (1998) 427–449.
[9] P. Zhao, W. Yuan, H. Sun, Y. Li, A.P. Kelley, X. Zheng, C.K. Law, Laminar flame speeds, counterflow ignition, and kinetic modeling of the butene isomers, Proc. Combust. Inst. 35 (2015) 309–316.
[10] K. Hoyermann, F. Mauß, T. Zeuch, A detailed chemical reaction mechanism for the oxidation of hydrocarbons and its application to the analysis of benzene formation in fuel-rich premixed laminar acetylene and propene flames, Phys. Chem. Chem. Phys. 6 (2004) 3824–3835.
[11] W.K. Metcalfe, S.M. Burke, S.S. Ahmed, H.J. Curran, A hierarchical and comparative kinetic modeling study of C1−C2 hydrocarbon and oxygenated fuels, Int. J. Chem. Kinet. 45 (2013) 638–675.
[12] H. Wang, X. You, A.V. Joshi, S.G. Davis, A. Laskin, F. Egolfopoulos, C.K. Law, High-temperature combustion reaction model of H2/CO/C1–C4 compounds, USC Mech Version II, 2007. http://ignis.usc.edu/USC_Mech_II.htm.
[13] N.M. Marinov, W.J. Pitz, C.K. Westbrook, A.M. Vincitore, M.J. Castaldi, S.M. Senkan, C.F. Melius, Aromatic and polycyclic aromatic hydrocarbon formation in a laminar premixed n-butane flame, Combust. Flame 114 (1998) 192–213.
[14] W.J. Pitz, C.K. Westbrook, W.M. Proscia, F.L. Dryer, A comprehensive chemical kinetic reaction mechanism for the oxidation of n-butane, Symp. (Int.) Combust. 20 (1985) 831–843.
[15] W.J. Pitz, C.K. Westbrook, Chemical kinetics of the high pressure oxidation of n-butane and its relation to engine knock, Combust. Flame 63 (1986) 113–133.
[16] S.M. Burke, W. Metcalfe, O. Herbinet, F. Battin-Leclerc, F.M. Haas, J. Santner, F.L. Dryer, H.J. Curran, An experimental and modeling study of propene oxidation. Part 1: Speciation measurements in jet-stirred and flow reactors, Combust. Flame 161 (2014) 2765–2784.
[17] S.M. Burke, U. Burke, R. Mc Donagh, O. Mathieu, I. Osorio, C. Keesee, A. Morones, E.L. Petersen, W. Wang, T.A. DeVerter, M.A. Oehlschlaeger, B. Rhodes, R.K. Hanson, D.F. Davidson, B.W. Weber, C.-J. Sung, J. Santner, Y. Ju, F.M. Haas, F.L. Dryer, E.N. Volkov, E.J.K. Nilsson, A.A. Konnov, M. Alrefae, F. Khaled, A. Farooq, P. Dirrenberger, P.-A. Glaude, F. Battin-Leclerc, H.J. Curran, An experimental and modeling study of propene oxidation. Part 2: Ignition delay time and flame speed measurements, Combust. Flame 162 (2015) 296–314.
[18] C.-W. Zhou, Y. Li, E. O'Connor, K.P. Somers, S. Thion, C. Keesee, O. Mathieu, E.L. Petersen, T.A. DeVerter, M.A. Oehlschlaeger, G. Kukkadapu, C.-J. Sung, M. Alrefae, F. Khaled, A. Farooq, P. Dirrenberger, P.-A. Glaude, F. Battin-Leclerc, J. Santner, Y. Ju, T. Held, F.M. Haas, F.L. Dryer, H.J. Curran, A comprehensive experimental and modeling study of isobutene oxidation, Combust. Flame 167 (2016) 353–379.
[19] Y. Li, C.-W. Zhou, K.P. Somers, K. Zhang, H.J. Curran, The oxidation of 2-butene: A high pressure ignition delay, kinetic modeling study and reactivity comparison with isobutene and 1-butene, Proc. Combust. Inst. 36 (2017) 403–411.
[20] C. Morley, Gaseq, version 0.76, (2004).
[21] D. Darcy, C.J. Tobin, K. Yasunaga, J.M. Simmie, J. Würmel, W.K. Metcalfe, T. Niass, S.S. Ahmed, C.K. Westbrook, H.J. Curran, A high pressure shock tube study of n-propylbenzene oxidation and its comparison with n-butylbenzene, Combust. Flame 159 (2012) 2219–2232.
[22] E.L. Petersen, M.J.A. Rickard, M.W. Crofton, E.D. Abbey, M.J. Traum, D.M. Kalitan, A facility for gas- and condensed-phase measurements behind shock waves, Meas. Sci. Technol. 16 (2005) 1716–1729.
[23] Z. Zhang, E. Hu, L. Pan, Y. Chen, J. Gong, Z. Huang, Shock-tube measurements and kinetic modeling study of methyl propanoate ignition, Energy Fuels 28 (2014) 7194–7202.

[24] W.S. Affleck, A. Thomas, An opposed piston rapid compression machine for preflame reaction studies, Proc. Inst. Mech. Eng. 183 (1968) 365–387.
[25] L. Brett, J. Macnamara, P. Musch, J.M. Simmie, Simulation of methane autoignition in a rapid compression machine with creviced pistons, Combust. Flame 124 (2001) 326–329.
[26] Reaction Design, CHEMKIN-PRO 15101, Reaction Design, San Diego, 2010.
[27] C.K. Westbrook, W.J. Pitz, J.E. Boercker, H.J. Curran, J.F. Griffiths, C. Mohamed, M. Ribaucour, Detailed chemical kinetic reaction mechanisms for autoignition of isomers of heptane under rapid compression, Proc. Combust. Inst. 29 (2002) 1311–1318.
[28] S. Tanaka, F. Ayala, J.C. Keck, A reduced chemical kinetic model for HCCI combustion of primary reference fuels in a rapid compression machine, Combust. Flame 133 (2003) 467–481.
[29] M. Ribaucour, R. Minetti, L.R. Sochet, H.J. Curran, W.J. Pitz, C.K. Westbrook, Ignition of isomers of pentane: an experimental and kinetic modeling study, Proc. Combust. Inst. 28 (2000) 1671–1678.
[30] Y. Zhao, D.G. Truhlar, The M06 suite of density functionals for main group thermochemistry, thermochemical kinetics, noncovalent interactions, excited states, and transition elements: two new functionals and systematic testing of four M06-class functionals and 12 other functionals, Theor. Chem. Acc. 120 (2008) 215–241.
[31] M.J. Frisch, G.W. Trucks, H.B. Schlegel, G.E. Scuseria, M.A. Robb, J.R. Cheeseman, G. Scalmani, V. Barone, B. Mennucci, G.A. Petersson, H. Nakatsuji, M. Caricato, X. Li, H.P. Hratchian, A.F. Izmaylov, J. Bloino, G. Zheng, J.L. Sonnenberg, M. Hada, M. Ehara, K. Toyota, R. Fukuda, J. Hasegawa, M. Ishida, T. Nakajima, Y. Honda, O. Kitao, H. Nakai, T. Vreven, J.A. Montgomery Jr., J.E. Peralta, F. Ogliaro, M. Bearpark, J.J. Heyd, E. Brothers, K.N. Kudin, V.N. Staroverov, R. Kobayashi, J. Normand, K. Raghavachari, A. Rendell, J.C. Burant, S.S. Iyengar, J. Tomasi, M. Cossi, N. Rega, J.M. Millam, M. Klene, J.E. Knox, J.B. Cross, V. Bakken, C. Adamo, J. Jaramillo, R. Gomperts, R.E. Stratmann, O. Yazyev, A.J. Austin, R. Cammi, C. Pomelli, J.W. Ochterski, R.L. Martin, K. Morokuma, V.G. Zakrzewski, G.A. Voth, P. Salvador, J.J. Dannenberg, S. Dapprich, A.D. Daniels, O. Farkas, J.B. Foresman, J.V. Ortiz, J. Cioslowski, D.J. Fox, Gaussian 09, Revision A.02, Gaussian, Inc., Wallingford CT, 2009.
[32] J.M.L. Martin, Ab initio total atomization energies of small molecules—towards the basis set limit, Chem. Phys. Lett. 259 (1996) 669–678.
[33] D. Feller, D.A. Dixon, Extended benchmark studies of coupled cluster theory through triple excitations, J. Chem. Phys. 115 (2001) 3484–3496.
[34] S. Glasstone, K.J. Laidler, H. Eyring, Theory of rate processes, McGraw-Hill, New York, 1941.
[35] C. Eckart, The penetration of a potential barrier by electrons, Phys. Rev. 35 (1930) 1303–1309.
[36] A.Y. Chang, J.W. Bozzelli, A.M. Dean, Kinetic analysis of complex chemical activation and unimolecular dissociation reactions using QRRK theory and the modified strong collision approximation, Z. Phys. Chem. 214 (2000) 1533–1568.
[37] P.R. Westmoreland, J.B. Howard, J.P. Longwell, A.M. Dean, Prediction of rate constants for combustion and pyrolysis reactions by bimolecular QRRK, AIChE J. 32 (1986) 1971–1979.
[38] S.W. Benson, Thermochemical kinetics, Wiley, 1976.
[39] S.M. Burke, J.M. Simmie, H.J. Curran, Critical evaluation of thermochemical properties of C1–C4 species: updated group-contributions to estimate thermochemical properties, J. Phys. Chem. Ref. Data 44 (2015) 013101.
[40] E.R. Ritter, J.W. Bozzelli, THERM: thermodynamic property estimation for gas phase radicals and molecules, Int. J. Chem. Kinet. 23 (1991) 767–778.
[41] A. Kéromnès, W.K. Metcalfe, K.A. Heufer, N. Donohoe, A.K. Das, C.-J. Sung, J. Herzler, C. Naumann, P. Griebel, O. Mathieu, M.C. Krejci, E.L. Petersen, W.J. Pitz, H.J. Curran, An experimental and detailed chemical kinetic modeling study of hydrogen and syngas mixture oxidation at elevated pressures, Combust. Flame 160 (2013) 995–1011.
[42] U. Burke, K.P. Somers, P. O'Toole, C.M. Zinner, N. Marquet, G. Bourque, E.L. Petersen, W.K. Metcalfe, Z. Serinyel, H.J. Curran, An ignition delay and kinetic modeling study of methane, dimethyl ether, and their mixtures at high pressures, Combust. Flame 162 (2015) 315–330.
[43] K.P. Somers, J.M. Simmie, F. Gillespie, C. Conroy, G. Black, W.K. Metcalfe, F. Battin-Leclerc, P. Dirrenberger, O. Herbinet, P.-A. Glaude, P. Dagaut, C. Togbé, K. Yasunaga, R.X. Fernandes, C. Lee, R. Tripathi, H.J. Curran, A comprehensive experimental and detailed chemical kinetic modelling study of 2,5-dimethylfuran pyrolysis and oxidation, Combust. Flame 160 (2013) 2291–2318.
[44] S.S. Vasu, L.K. Huynh, D.F. Davidson, R.K. Hanson, D.M. Golden, Reactions of OH with butene isomers: measurements of the overall rates and a theoretical study, J. Phys. Chem. A 115 (2011) 2549–2556.
[45] J. Zador, A.W. Jasper, J.A. Miller, The reaction between propene and hydroxyl, Phys. Chem. Chem. Phys. 11 (2009) 11040–11053.
[46] J.-C. Loison, J. Daranlot, A. Bergeat, F. Caralp, R. Mereau, K.M. Hickson, Gas-phase kinetics of hydroxyl radical reactions with C_3H_6 and C_4H_8: product branching ratios and OH addition site-specificity, J. Phys. Chem. A 114 (2010) 13326–13336.
[47] J.D. DeSain, S.J. Klippenstein, J.A. Miller, C.A. Taatjes, Measurements, theory, and modeling of OH formation in ethyl + O_2 and propyl + O_2 reactions, J. Phys. Chem. A 107 (2003) 4415–4427.
[48] C.F. Goldsmith, W.H. Green, S.J. Klippenstein, Role of O2 + QOOH in low-temperature ignition of propane. 1. Temperature and pressure dependent rate coefficients, J. Phys. Chem. A 116 (2012) 3325–3346.
[49] W. Tsang, Chemical kinetic data base for combustion chemistry. Part V. Propene, J. Phys. Chem. Ref. Data 20 (1991) 221–273.
[50] A. Miyoshi, Systematic computational study on the unimolecular reactions of alkylperoxy (RO_2), hydroperoxyalkyl (QOOH), and hydroperoxyalkylperoxy (O_2QOOH) radicals, J. Phys. Chem. A 115 (2011) 3301–3325.
[51] H. Sun, J.W. Bozzelli, C.K. Law, Thermochemical and kinetic analysis on the reactions of O_2 with products from OH addition to isobutene, 2-hydroxy-1,1-dimethylethyl, and 2-hydroxy-2-methylpropyl radicals: HO_2 formation from oxidation of neopentane, part II, J. Phys. Chem. A 111 (2007) 4974–4986.
[52] W. Tsang, R.F. Hampson, Chemical kinetic data base for combustion chemistry. Part I. Methane and related compounds, J. Phys. Chem. Ref. Data 15 (1986) 1087–1279.
[53] J. Zádor, S.J. Klippenstein, J.A. Miller, Pressure-dependent OH Yields in alkene + HO_2 reactions: a theoretical study, J. Phys. Chem. A 115 (2011) 10218–10225.
[54] S.M. Villano, H.-H. Carstensen, A.M. Dean, Rate rules, branching ratios, and pressure dependence of the HO_2 + olefin addition channels, J. Phys. Chem. A 117 (2013) 6458–6473.
[55] S. Sharma, S. Raman, W.H. Green, Intramolecular hydrogen migration in alkylperoxy and hydroperoxyalkylperoxy radicals: accurate treatment of hindered rotors, J. Phys. Chem. A 114 (2010) 5689–5701.
[56] S.M. Villano, L.K. Huynh, H.-H. Carstensen, A.M. Dean, High-pressure rate rules for alkyl + O_2 reactions. 2. The isomerization, cyclic ether formation, and β-scission reactions of hydroperoxy alkyl radicals, J. Phys. Chem. A 116 (2012) 5068–5089.
[57] S.M. Villano, L.K. Huynh, H.-H. Carstensen, A.M. Dean, High-pressure rate rules for alkyl+O_2 reactions. 1. The dissociation, concerted elimination, and isomerization channels of the alkyl peroxy radical, J. Phys. Chem. A 115 (2011) 13425–13442.
[58] A. Miyoshi, Molecular size dependent falloff rate constants for the recombination reactions of alkyl radicals with O_2 and implications for simplified kinetics of alkylperoxy radicals, Int. J. Chem. Kinet. 44 (2012) 59–74.
[59] J.A. Miller, S.J. Klippenstein, From the multiple-well master equation to phenomenological rate coefficients: reactions on a C_3H_4 potential energy surface, J. Phys. Chem. A 107 (2003) 2680–2692.
[60] J.A. Miller, S.J. Klippenstein, Master equation methods in gas phase chemical kinetics, J. Phys. Chem. A 110 (2006) 10528–10544.
[61] A. Fridlyand, P.T. Lynch, R.S. Tranter, K. Brezinsky, Single pulse shock tube study of allyl radical recombination, J. Phys. Chem. A 117 (2013) 4762–4776.
[62] M.M. Kopp, N.S. Donato, E.L. Petersen, W.K. Metcalfe, S.M. Burke, H.J. Curran, Oxidation of ethylene–air mixtures at elevated pressures, part 1: Experimental Results, J. Propul. Power 30 (2014) 790–798.
[63] M.M. Kopp, E.L. Petersen, W.K. Metcalfe, S.M. Burke, H.J. Curran, Oxidation of ethylene—air mixtures at elevated pressures, part 2: chemical kinetics, J. Propul. Power 30 (2014) 799–811.
[64] C.F. Goldsmith, L.B. Harding, Y. Georgievskii, J.A. Miller, S.J. Klippenstein, Temperature and pressure-dependent rate coefficients for the reaction of vinyl radical with molecular oxygen, J. Phys. Chem. A 119 (2015) 7766–7779.
[65] S.M. Sarathy, S. Vranckx, K. Yasunaga, M. Mehl, P. Oßwald, W.K. Metcalfe, C.K. Westbrook, W.J. Pitz, K. Kohse-Höinghaus, R.X. Fernandes, H.J. Curran, A comprehensive chemical kinetic combustion model for the four butanol isomers, Combust. Flame 159 (2012) 2028–2055.
[66] D.J.M. Ray, D.J. Waddington, Gas phase oxidation of alkenes—Part II. The oxidation of 2-methylbutene-2 and 2,3-dimethylbutene-2, Combust. Flame 20 (1973) 327–334.
[67] M.I. Sway, D.J. Waddington, Reactions of oxygenated radicals in the gas phase. Part 12. The reactions of isopropylperoxyl radicals and alkenes, J. Chem. Soc., Perkin Trans. 2 (1983) 139–143.